

**UNIVERSITY OF GAZ ANTEP
GRADUATE SCHOOL OF
NATURAL & APPLIED SCIENCES**

**REPEATABILITY OF SELF-HEALING IN CEMENTITIOUS
COMPOSITES**

**M. Sc. THESIS
IN
CIVIL ENGINEERING**

**BY
REZHIN AZAD NOORI
NOVEMBER 2013**

Repeatability of Self-Healing in Cementitious Composites

**M.Sc. Thesis
in
Civil Engineering
University of Gaziantep**

**Supervisors
Assoc. Prof. Dr. Mustafa ŞAHMARAN
Prof. Dr. Mustafa GÜNAL**

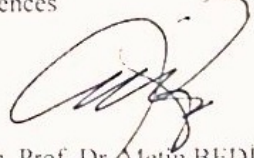
**by
Rezhin AZAD NOORI
November 2013**

© 2013 [Rezhin AZAD NOORI]


T.C.
UNIVERSITY OF GAZIANTEP
GRADUATE SCHOOL OF
NATURAL & APPLIED SCIENCES
CIVIL ENGINEERING DEPARTMENT

Name of the thesis: Influence of Physical Parameters on Self-Healing Capability of
Cementitious Composites
Name of the student: Rezhin Azad NOORI
Exam date: 19.11.2013

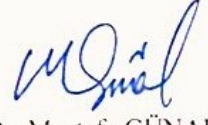
Approval of the Graduate School of Natural and Applied Sciences



Assoc. Prof. Dr. Metin BEDIR
Director

I certify that this thesis satisfies all the requirements as a thesis for the degree of
Master of Science.


Prof. Dr. Mustafa GÜNAL
Head of Department

This is to certify that we have read this thesis and that in our opinion it is fully
adequate, in scope and quality, as a thesis for the degree of Master of Science.


Prof. Dr. Mustafa GÜNAL
Co-Supervisor


Assoc. Prof. Dr. Mustafa ŞAHMARAN
Supervisor

Examining Committee Members

Signature

Assoc. Prof. Dr. Aytaç GÜVEN

Assist. Prof. Dr. Ömer PAYDAK

Assoc. Prof. Dr. Mustafa ŞAHMARAN





I hereby declare that all information in this document has been obtained and presented in accordance with academic rules and ethical conduct. I also declare that, as required by these rules and conduct, I have fully cited and referenced all material and results that are not original to this work.

Rezhin Azad NOORI

ABSTRACT

REPEATABILITY OF SELF-HEALING IN CEMENTITIOUS COMPOSITES

NOORI, Rezhin Azad

M.Sc. in Civil Engineering

Supervisor: Assoc. Prof. Dr. Mustafa ŞAHMARAN

November 20 13, 61 pages

In this paper, intrinsic self-healing ability of Engineered Cementitious Composites (ECC) was investigated in terms of two robustness criteria; repeatability and pervasiveness. To do this, different composites with Class-F fly ash (F_ECC) and slag (S_ECC) were examined. In order to generate microcracks, specimens were repeatedly pre-loaded up to 70% of their deformation capacities under splitting tensile loading and exposed to cyclic wet/dry conditioning thereafter. Resonant frequency (RF) and rapid chloride permeability tests (RCPT) were utilized to assess the extent of damage and final results were supported by the microscopic observations. RF measurements were recorded from two different parts of the specimens to monitor if self-healing was pervasive. Results show that depending on the type of mineral additive and initial curing time, ECC specimens can recover up to 85% of their initial RF values even after six repetitive pre-loading. Although, the extent is slightly less, the recovery rates observed from the middle portions are similar to those observed from the top portion of the all ECC mixtures implying that self-healing is quite pervasive. After the application of severe pre-loading for five times, RCPT results of both mixtures satisfy low chloride ion penetrability levels. Maximum crack width observed over the specimen surfaces is restricted to 190 μm level even after nine repetitive pre-loading. These findings suggest that under certain conditions ECC materials produced in this study may significantly enhance the functionality of structures by further reducing the repair and/or maintenance need.

Keywords: Engineered Cementitious Composites (ECC); Self-Healing; Repeatability; Supplementary cementitious materials (SCM).

ÖZET

ÇİMENTO ESASLI KOMPOZİTLERDE KENDİLİĞİNDEN İYİLEŞMENİN TEKRARLANABİLİRLİĞİ

NOORI, Rezhin Azad
Mühendislik Yüksek Lisans
Tez Yöneticisi: Doç. Dr. Mustafa ŞAHMARAN
Kasım 2013, 61 sayfa

Bu çalışmada, tasarlanmış çimento esaslı kompozitlerin (ECC) kendiliğinden iyileşme özelliği tekrarlanabilirlik ve geniş alana yayılabilirlik olarak adlandırılan iki farklı kararlılık kriteri açısından incelenmiştir. Bunun için F-sınıfı uçucu kül (F-ECC) ve cüruf (S-ECC) içeren kompozitler üretilmiştir. Numuneler mikroçatlak oluşumu için yarmada çekme yüklemesi altında deformasyon kapasitelerinin %70'ine kadar tekrarlı önyüklemeye ve sonrasında ise çevrimsel ıslak/kuru kür koşuluna bırakılmıştır. Hasarın büyüklüğünün değerlendirilebilmesi için rezonans frekansı (RF) ve hızlı klorür geçirimsizliği (RCPT) testleri kullanılmış ve nihai sonuçlar mikroskobik gözlemlerle desteklenmiştir. Kendiliğinden iyileşmenin tüm numuneye yayılabilirliğinin anlaşılabilmesi için RF ölçümleri numunelerin iki farklı bölgesinden kaydedilmiştir. Sonuçlar, kullanılan mineral katkı ve kür süresine bağlı olarak, ECC numunelerinin tekrarlanan altı önyükleme sonrasında dahi ilk RF ölçümlerinin %85'ine kadar iyileşebildiğini göstermektedir. Oran az miktar düşse de, orta nokta ölçümlerindeki iyileşme üst nokta ölçümlerindeki iyileşmeye yakın bulunmuştur. Tekrarlanan beş önyüklemenin ardından, RCPT sonuçlarının tüm karışımlarda düşük seviyede kaldığı görülmüştür. Numunelerin en büyük çatlak genişliği, tekrarlanan dokuz önyükleme sonucunda dahi, 190 μ m seviyesinde kalmıştır. Sonuçlar, bu çalışmada üretilen ECC karışımlarının belirli koşullar altında, bakım ve/veya onarım ihtiyacını en aza indirgeyerek yapıların işlevselliğini önemli ölçüde iyileştirebileceğini göstermektedir.

AnahtarKelimeler: TasarlanmışÇimentoEsaslıKompozitler(ECC);

Kendiliğinden iyileşme; Tekrarlanabilirlik; lavebağlayıcımalzemeler (BM).

ACKNOWLEDGEMENT

This dissertation has been completed under the guidance of my advisor, Assoc. Prof. Dr. Mustafa ŞAHMARAN. Without his support, inspiration, dedication of time and energy throughout the past year, I could have never completed this work. I owe forever my sincerest gratitude to him, for opening my ideas to the innovative material technology world, and for challenging me with novel research ideas capable of solving real-world problems. I would also like to special thanks to my co-supervisor, Prof. Dr. Mustafa GÜNAL, for his support during this thesis with his knowledge and experiences.

I must acknowledge the financial assistance of the Scientific and Technical Council of Turkey (TÜB TAK) provided under project of MAG-112M876.

My deep appreciations and thanks to Res. Asst. Gürkan YILDIRIM and Assist. Prof. Dr. HasanErhan YUCEL for their helps and valuable suggestions.

I would also like to special thanks to Assoc. Prof. Dr. Aytaç GÜVEN and Asst. Prof. Dr. Ömer PAYDAK for serving on the committee.

Finally, I would also thanks to my family for their support and encouragement during my study.

TABLE OF CONTENTS

	Page
ABSTRACT	v
ÖZET	vi
ACKNOWLEDGEMENT	vii
TABLE OF CONTENTS	viii
LIST OF FIGURES	xi
LIST OF TABLES	xiv
LIST OF SYMBOLS/ABBREVIATIONS	xv
CHAPTER 1	1
INTRODUCTION	1
1.1 General	1
1.2 Research Objectives	3
CHAPTER 2	5
LITERATURE REVIEW AND BACKGROUND	5
2.1 Introduction	5
2.2 Engineered Cementitious Composites	7
2.3 Design of Engineered Cementitious Composites.....	9
2.4 Self-Healing Techniques in Cementitious Composites.....	12
2.4.1 Microencapsulation	12
2.4.2 Hollow Fibers	14
2.4.3 Bacteria Additive	18
2.4.4 Mineral Admixtures and Expansive Agents	20
2.5 Pozzolanic Material.....	22

2.5.1 Slag.....	23
2.5.2 Fly Ash	24
CHAPTER 3	26
EXPERIMENTAL PROGRAM	26
3.1 Materials.....	26
3.1.1 Cement	26
3.1.2 Fly Ash	27
3.1.3 Slag.....	27
3.1.4 Aggregate	28
3.1.5 Chemical Admixtures	29
3.1.6 Polyvinyl Alcohol (PVA) Fiber	29
3.2 ECC Mixing and Specimen Preparation	30
3.3 Pre-cracking and Self-Healing Evaluation Methods	33
3.4 Test Procedure.....	35
3.4.1 Resonant Frequency (RF)	35
3.4.2 Rapid Chloride Permeability Test (RCPT)	36
CHAPTER 4	37
RESULTS AND DISCUSSIONS	37
4.1 Resonant Frequency (RF) Test.....	37
4.1.1 Unhealed Specimens	37
4.1.2 Effects of Self-Healing.....	40
4.2 Rapid Chloride Permeability Test (RCPT)	43
4.2.1 Unhealed Specimens	43
4.2.2 Effects of Self-Healing.....	45
4.3 Crack Characteristics	47
CHAPTER 5	51

CONCLUSIONS	51
REFERENCES	53

LIST OF FIGURES

	Page
Figure 2.1 Possible mechanisms for self-healing in cementitious materials a) formation of calcium carbonate or calcium hydroxide, b) blocking cracks by impurities in the water and loose concrete particles resulting from crack spalling, c) further hydration of the unreacted cement or cementitious materials, d) expansion of the hydrated cementitious matrix in the crack flanks (swelling of C–S–H) (Schlangen, 2010)	6
Figure 2.2 Cracks filled with white residue a) the width of the specimen is 40 mm (Qian et al., 2009) b) crystallized products found in the cracks, the crack width is about 100 μm (Homma et al., 2009).....	7
Figure 2.3 Typical tensile stress-strain curve and crack width development of ECC (Weimann and Li, 2003)	9
Figure 2.4 Response of ECC under flexural loading	9
Figure 2.5 Crack bridging stress versus crack opening relation	10
Figure 2.6 a) Basic method of the microcapsule approach (Li and Herbert, 2012) b) ESEM image showing a ruptured microcapsule (White et al., 2001)	13
Figure 2.7 Schematic illustration of glass tubing self-healing approach approach (Li and Herbert, 2012)	14
Figure 2.8 Schematic diagram of external healing agent supply system (Mihashi et al., 2000)	15
Figure 2.9 Experimental configuration used throughout the tests (Joseph et al., 2007).....	16

Figure 2.10 Self-healing system of internal encapsulation method with hollow glass tubes (a) middle section view (b) side view (c) epoxy-filled glass tube with aquastick as sealant (Thao et al., 2009).....	17
Figure 2.11 Schematic illustration of bacteria additive self-healing approach (Li and Herbert, 2012).....	18
Figure 2.12 ESEM images showing self-healing activity through calcium carbonate formation with scale bars of a) 100 μm , b) 50 μm (Van der Zwaag, 2010).....	20
Figure 2.14 ESEM image of healing products. (a) Comparison between geopolymeric gel phase from self-healing area and hydrogarnet phase from original area (b) formation of hydrogarnet phases, AFt phases and calcite in self-healing zone (Ahn and Kishi, 2008)	22
Figure 3.1 Particle size distributions of sand, portland cement, fly as h and slag	27
Figure 3.2 Particle morphology of a) Class-F fly ash b) slag determined by SEM ...	28
Figure 3.3 A view of quartz sand aggregate	28
Figure 3.4 PVA Fiber used in the production of ECC	29
Figure 3.5 Typical flexural stress – mid-span deflection curves of ECC mixtures at age of 28 days.....	31
Figure 3.6 Production of ECC by using Hobart Type mixer	32
Figure 3.7 Splitting tensile strength test setup	34
Figure 3.8 Observation of cracks under a) portable microscope b) video microscope	35
Figure 3.9 a) View of resonant frequency test (RF) set up b) schematic representation of resonant frequency test setup	36

Figure 3.10 Rapid chloride permeability test (RCPT) setup	36
Figure 4.1 Percent variations in RF measurements due to repetitive pre-loading and subsequent conditioning	39
Figure 4.2 Percent variations in chloride ion permeability values of ECC mixtures due to repetitive pre-loading and subsequent conditioning.....	44
Figure 4.3 Total crack closure rates of ECC specimens in percentage	49

LIST OF TABLES

	Page
Table 2.1 Typical mix design of ECC material.....	8
Table 2.2 Specifications for fly ash (ASTM C 618, 2003)	25
Table 3.1 Chemical and physical properties of portland cement, fly ash and slag	26
Table 3.2 Mechanic and Geometric Properties of PVA Fibers.....	30
Table 3.3 ECC mixture proportions	31
Table 4.1 Rapid chloride permeability test results of ECC specimens	43
Table 4.2 Crack characteristics of pre-loaded ECC specimens	48

LIST OF SYMBOLS/ABBREVIATIONS

P_e	Applied load
$f\left(\frac{a}{W}\right)$	Geometric calibration factor
C-S-H	Calcium silicate hydrate
ECC	Engineered cementitious composites
$e^{f\phi}$	Accounts for the changes in bridging force for fibers crossing at an inclined angle to the crack plane
ESEM	Environmental scanning electron microscopy
F	Class-F fly ash
f	Snubbing coefficient
F_ECC	Class-F fly ash incorporating ECC
FRC	Fiber reinforced concrete
HRWRA	High range water reducing admixture
J'_b	Complimentary energy
J_{tip}	Fracture energy of the mortar matrix
K_m	Fracture toughness of the mortar matrix
L_f	Fiber length
MA/CM	Mineral admixture to cementitious materials ratio
MAS	Maximum aggregate size

$p(z)$	Centroidal distance from the crack plane
$P(\delta)$	Pullout load versus displacement relation of a single fiber aligned normal to the crack plane
$p(\phi)$	Probability density functions of the fiber orientation angle
PC	Portland cement
PVA	Poly-vinyl-alcohol
RCPT	Rapid chloride permeability test
RF	Resonant frequency
S	Ground granulated blast furnace slag
S/C	Slag to cement ratio
S_ECC	Slag incorporating ECC
SEM	Scanning electron microscopy
V_f	Fiber volume fraction
W/CM	Water to cementitious materials ratio
W/D	Wet-dry conditioning
z	Centroidal distance of a fiber from the crack plane
δ_0	Crack opening
ϕ	Orientation angle of the fiber
σ_0	Maximum crack bridging stress
σ_{fc}	First cracking strength of the mortar matrix

CHAPTER 1

INTRODUCTION

1.1 General

It is highly desirable that concrete material used in civil infrastructures should last for a long time period without sacrificing the durability properties. However, due to several deteriorating mechanisms, concrete unavoidably cracks which may lead to the emergence of more severe degradation processes and significant reductions in service life. Such damages frequently require repeated maintenance and/or repair of degraded section in order to compensate the performance lack. However, it is reported that repairs are often short-lived and half of the repairs applied in fields fail (Mather and Warner, 2003). To make matters worse, the implementation of continuous maintenance and/or repair works is not always feasible especially in the case of large-scale concrete infrastructures mainly due to significantly increased labor and capital necessity. In addition, owing to structural restrictions and conditions, repairing can be difficult or even impossible to execute in some cases. Under such circumstances, self-repair or rather self-healing of concrete material without external human interference could be of great attraction.

Up to date, many researchers have already engaged in emerging techniques in order to functionalize the self-healing ability of cracked concrete. Such innovative techniques can be counted as the utilization of hollow fibers, (Mihashi et al., 2000) chemical and bacterial encapsulation, (Huang and Ye, 2011; Jonkers, 2011) expansive agents and mineral admixtures, (Kishi et al., 2007; Ahn and Kishi, 2010) and intrinsic self-healing with self-controlled tight crack width (Sahmaran et al., 2012). Although, all of the approaches listed above unarguably hold promise, several concerns still exist related to the robustness of self-healing mechanism (Li and Herbert, 2012). One of such concerns is the repeatability of self-healing phenomenon. It is likely to say that over the lifetime of an infrastructure, damage occurrence will take place more than once due to several overloading conditions. The

possible relapse of the overloading conditions usually requires multiple occurrence of self-healing of cracks in the structures. This therefore implies that self-healing capability of structures should be repeatable in order to satisfy the functionality of the structures even in the cases where crack opening occurs from the same location of a known place. Another concern related to self-healing robustness arises due to the complexity of different loading types over structures. Since it is not always easy to presume the place where cracking will take place and how the crack orientation will be, healing that is pervasive rather than only present in discrete parts of the structures is extremely appealing. Although, the aforementioned self-healing approaches are limitedly effective in fulfilling several robustness criteria, the utilization of intrinsic self-healing which is coupled with the formation of many closely spaced multiple microcracks over the concrete seems to be the most promising technique if repeatability and pervasiveness of the self-healing mechanism are of concern (Li and Herbert, 2012). The dependence of self-healing on tight crack widths, likely less than 150 μm , was already shown by previous studies (Edvardsen, 1999; Jacobsen et al., 1995; Reinhardt and Jooss, 2003). This is very difficult to achieve in the case of conventional concrete. Therefore, the possibility to attain consistent and robust self-healing behavior with conventional concrete is rather small. However, a newly-developed material called Engineered Cementitious Composites (ECC) contributes much more to the self-healing behavior than normal concrete with its superior characteristics.

Engineered Cementitious Composites (ECC) is one of the special branch of high performance-fiber reinforced cementitious composites developed in the last decades. The optimization of ECC has been supplied through the application of micromechanics-based design theory in order to attain high tensile ductility and tight microcrack formation under direct tension at moderate fiber contents (2% by volume, or less) (Lin et al., 1999; Lin and Li 1997; Li, 1997). The extreme ductility of ECC is several hundred times that of conventional and fiber reinforced concrete (FRC). Increased ductility leads ECC materials to exhibit exceptional enhancement in toughness values which is quite similar to that of metals (Maalej et al, 1995). Along with the improvement in toughness values, average crack widths remain at about 60 μm level regardless of the ultimate tensile strain. This behavior is provided by the occurrence of steady-state “flat cracks” that has constant crack widths irrespective of

the crack length, by contrast with most FRC materials showing Griffith-type cracks which widen as cracks grow (Li, 1998; Li, 2003; Li et al., 2001).

Augmentation of human population and industrialization bring along increasing concerns related to raw material diminishment, global warming and climate change. One of the aspects contributing to ever-increasing concerns is cement production which is the main cause of nearly 7% of total worldwide emissions from industrial sources. In this regard, incorporating sustainability issues into the design of civil engineering materials is of the essence. Utilization of supplementary cementitious materials (SCM) as a partial replacement of cement stands as one plausible way to reduce the environmental impact caused due to cement manufacture. In addition, partial replacement of portland cement with SCMs (i.e. fly ash, slag etc.) can lower the material cost, reduce environmental burden and enhance the greenness, since the production of these materials needs less energy and causes less carbon dioxide emission than cement. Along with environmental benefits, it is reported that usage of high volumes of fly ash rehabilitates the robustness of ECC by improving tensile ductility and contributes self-healing behavior by reducing crack widths approximately from 60 μm level to 10-30 μm level or sometimes even lower than 10 μm levels (Yang et al., 2007; Wang and Li, 2007, Sahmaran and Li, 2007). Furthermore, in the cases where high volumes of SCMs are used in the concrete mixtures, contingency for self-healing to occur is expected to increase since much of these materials remain unhydrated for a longer time period.

1.2 Research Objectives

In the present thesis, ECC mixtures incorporating high volumes of different SCMs were produced to take dual advantage of material greenness and further self-healing probability. Throughout the study, concentration was mainly placed upon the observation of self-healing phenomenon in terms of repeatability and pervasiveness. Two test methods; resonant frequency (RF) and rapid chloride permeability (RCPT), were introduced and recovery in the results were compared after repeated pre-loading and subsequent cyclic environmental conditioning. In order to assess whether the self-healing extends over the entire area of specimens or not, RF measurements taken

from different parts of specimens were compared. Additionally, the results were supported by the observations made on crack width measurements.

In Chapter 2, a detailed literature review on subjects related to the main idea of the present thesis was given. In Chapter 3, experimental program, properties of the materials and details of the tests performed to assess the self-healing capability in terms of repeatability and pervasiveness were presented. The results of the experimental studies are presented and discussed in Chapter 4. The conclusions of the research are represented in Chapter 5.

CHAPTER 2

LITERATURE REVIEW AND BACKGROUND

2.1 Introduction

Due to its significantly low cost and relatively high compressive strength, concrete is the mostly preferred construction materials all over the world. Concrete shows superior compressive characteristics however it is substantially weak when exposed to tensile forces which makes the utilization of steel reinforcement indispensable during the construction of real-life structures. Although, the incorporation of rebars restricts the cracks with wider widths, they do not prevent the crack formation entirely. Durability of the structures are significantly influenced by the formation cracks since the penetration of aggressive liquids, ions and gasses would be penetrated easily to the matrix itself and lead to overall damage. As a result, cracks may get larger and the reinforcing steel could be subjected to the environmental effects. With the commencement of rebar corrosion, structure may collapse entirely. This therefore implies that repair and/or maintenance or at least the inspection of cracks is highly desirable. Although the repairment of cracks is highly important, the implementation of the process is rather difficult in the cases where cracks are not visible and easily accessible. In addition to the direct expenses, several other problems such as traffic jams, delays in serviceability and so on may arise as a result of repair applications. Along these lines self-healing of concrete material could be of great significance. Under such conditions, automatic repair or rather self-healing of cracks could be of interest to many.

The inspiration for the development of artificial self-healing materials fundamentally comes from the nature. Autonomous healing of damaged skins of trees, animals or humans in time can be given as a principle example for the self-healing phenomenon. The discovery of self-healing or autogenous healing of cracked concrete was first observed in eighteenth century in water retaining structures, culverts and pipes (Hearn and Morley, 1997). At the end of nineteenth century was also studied by

several researchers (Hearn and Morley, 1998; Hyde and Smith, 1889). Glanville (1931) was one of the first making a systematic study related to the self-healing phenomenon back in 1926. The differences between self-healing and self-sealing were already set at that time so that in the former complete compressive strength recovery was obtained while in the latter only leakage was restricted with no strength recovery. Self-healing was also observed in the case of specimens exposed to freezing and thawing effect (Jacobsen and Sellevold, 1996). Moreover, extensive studies were undertaken related to self-healing of leaking cracks by several authors (Clear, 1985; Hearn, 1999; Edvardsen, 1999; Hearn and Morley, 1997; Hearn and Morley, 1998). Experimental studies and years of experience show that self-healing phenomenon observed in cementitious materials is a consequence of several physical and chemical processes. The possible mechanisms that could contribute to the occurrence of self-healing was schematically shown in Figure 2.1 (Schlangen, 2010).

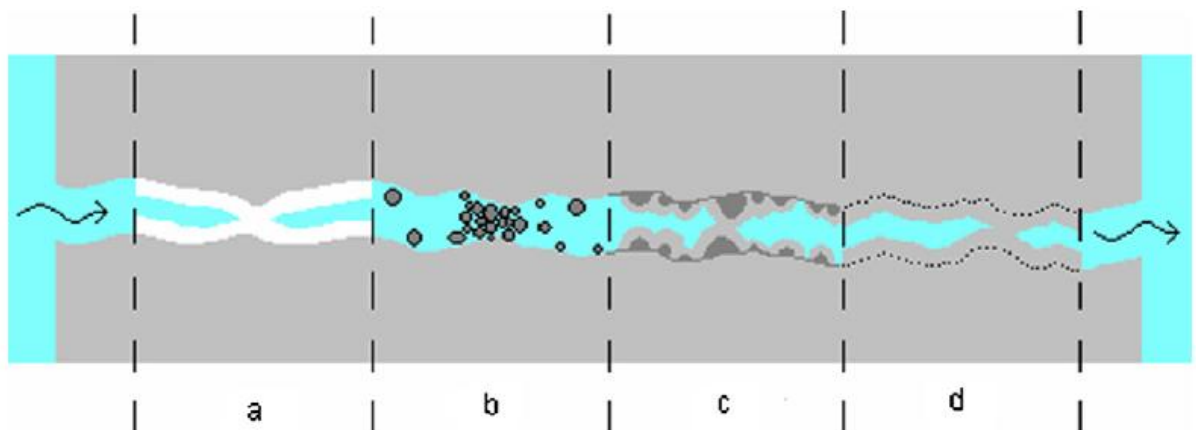


Figure 2.1 Possible mechanisms for self-healing in cementitious materials a) formation of calcium carbonate or calcium hydroxide, b) blocking cracks by impurities in the water and loose concrete particles resulting from crack spalling, c) further hydration of the unreacted cement or cementitious materials, d) expansion of the hydrated cementitious matrix in the crack flanks (swelling of C-S-H) (Schlangen, 2010)

Although all of the mechanism mentioned above could be responsible for the occurrence of self-healing, the primary cause is attributed to the formation of calcium carbonate. (Edvardsen, 1999; Yang et al., 2007). This finding was also supported with the fact that calcium carbonate precipitation is generally observed as white residue over a healed concrete surface which is shown in Figure 2.2-a macroscopically and Figure 2.2-b microscopically.



(a)

(b)

Figure 2.2 Cracks filled with white residue a) the width of the specimen is 40 mm (Qian et al., 2009) b) crystallized products found in the cracks, the crack width is about 100 μm (Homma et al., 2009)

According to Neville, self-healing phenomenon was attributed to the further hydration of unhydrated cementitious materials present in the matrix itself (Neville, 1996). However, then it was concluded that this situation holds only true for very young concrete and self-healing observed in the later ages was mostly related with the calcium carbonate formation. (Neville, 2002).

2.2 Engineered Cementitious Composites

As a new class of High Performance Fiber Reinforced Cementitious Composites (HPFRCC) materials, Engineered Cementitious Composites (ECC) is a ductile fiber reinforced cementitious composite micromechanically designed to achieve high damage tolerance under severe loading and high durability under normal service conditions (Li, 1998; Li et al., 2001; Li, 2003). The most distinctive characteristic separating ECC from conventional concrete and fiber reinforced concrete (FRC) is an ultimate tensile strain capacity between 3% to 5%, depending on the specific ECC mixture. This strain capacity is realized through the formation of many closely spaced microcracks, allowing for a strain capacity over 300 times that of normal concrete. These cracks, which carry increasing load after formation, allow the material to exhibit strain hardening, similar to many ductile metals.

While the components of ECC may be similar to FRC, the distinctive ECC characteristic of strain hardening through microcracking is achieved through

micromechanical tailoring of the components (i.e. cement, aggregate, and fibers) (Li, 1998; Lin et al., 1999; Li et al., 2001; Li, 2003), along with control of the interfacial properties between components. Fracture properties of the cementitious matrix are carefully controlled through mix proportions. Fiber properties, such as strength, modulus of elasticity, and aspect ratio have been customized for use in ECC. The interfacial properties between fiber and matrix have also been optimized in cooperation with the manufacturer for use in this material. Typical mix proportions of ECC using a poly-vinyl-alcohol (PVA) fiber are given in Table 2.1.

Table 2.1 Typical mix design of ECC material

Cement	1.00
Water	0.58
Aggregate	0.80
Fly Ash	1.20
HRWR*	0.013
Fiber (%)	2.00

*HRWR = High range water reducing admixture; all ingredients proportion by weight except for fiber.

While most HPFRCCs rely on a high fiber volume to achieve high performance, ECC uses low amounts, typically 2% by volume, of short, discontinuous fiber. This low fiber volume, along with the common components, allows flexibility in construction execution. To date, ECC materials have been engineered for self-consolidation casting (Kong et al., 2003), extrusion (Stang and Li, 1999), shotcreting (Kim et al., 2003), and conventional mixing in a gravity mixer or conventional mixing truck (Lepech and Li, 2008).

Figure 2.3 shows a typical uniaxial tensile stress-strain curve of ECC material containing 2% poly-vinyl-alcohol (PVA) fiber (Weimann and Li, 2003). The characteristic strain-hardening behavior after first cracking is accompanied by multiple microcracking. The crack width development during inelastic straining is also shown in Figure 2.3. Even at ultimate load, the crack width remains smaller than 80 μm . This tight crack width is self-controlled and, whether the composite is used in combination with conventional reinforcement or not, it is a material characteristic independent of rebar reinforcement ratio. In contrast, normal concrete and fiber reinforced concrete rely on steel reinforcement for crack width control. Under severe

bending loads, an ECC beam deforms similar to a ductile metal plate through plastic deformation (Figure 2.4). In compression, ECC materials exhibit compressive strengths similar to high strength concrete (e.g. greater than 60 MPa) (Lepech and Li, 2008).

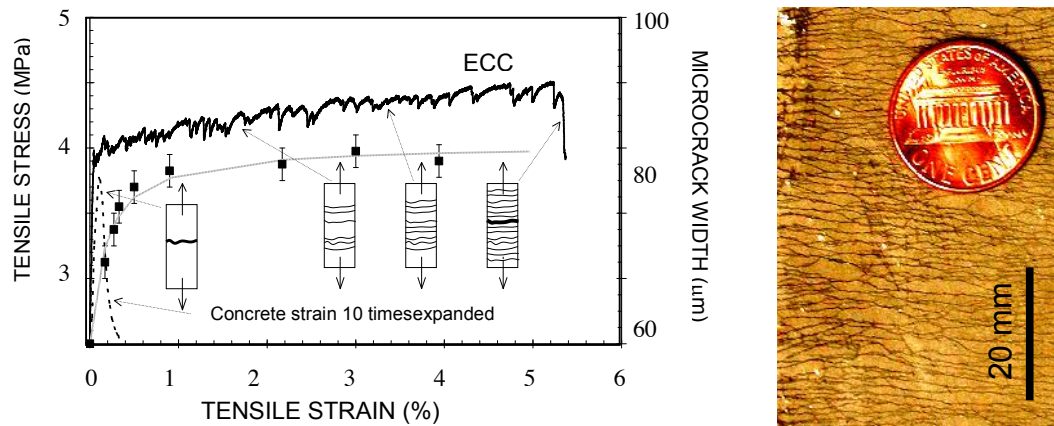


Figure 2.3 Typical tensile stress-strain curve and crack width development of ECC (Weimann and Li, 2003)



Figure 2.4 Response of ECC under flexural loading

2.3 Design of Engineered Cementitious Composites

In design of ECC material, primary purpose is to assure the occurrence of multiple cracking and strain hardening behavior under loading. Through the formation of multiple microcracks, large deformations are easy to be experienced over the span of specimen. Marshall and Cox (1988) first stated that, the formation of multiple microcracking and strain hardening behavior in ECC is dependent on steady state cracks to propagate. This finding then extended by Li and Leung (1992) and Lin et

al. (1999) to be used in the case of fiber reinforced cementitious composites. Instead of Griffith-type cracks that open up while propagating as in typical tension-softening fiber reinforced cementitious materials, ECC material experiences large tensile strains in the strain hardening stage through the saturation of specimen with steady state “flat cracks” that keep crack width constant during the propagation. Fiber bridging stress versus crack width opening relation and the cracking toughness of mortar matrix are two main criteria that are responsible for the occurrence of multiple steady state cracking behavior. In order to obtain this behavior the inequality shown in Equation-2.1 must be fulfilled.

$$J'_b = \sigma_0 \delta_0 - \int_0^{\delta_0} \sigma(\delta) d\delta \geq J_{tip} \approx \frac{K_m^2}{E_m} \quad (2.1)$$

where J'_b is the complimentary energy shown in Figure 2.5, σ_0 and δ_0 are the maximum crack bridging stress and corresponding crack opening, J_{tip} is the fracture energy of the mortar matrix, K_m is the fracture toughness of the mortar matrix, and E_m is the elastic modulus of the mortar matrix. In addition to the fracture energy criterion, a strength criterion expressed in Equation-2.2 must be satisfied.

$$\sigma_0 > \sigma_{fc} \quad (2.2)$$

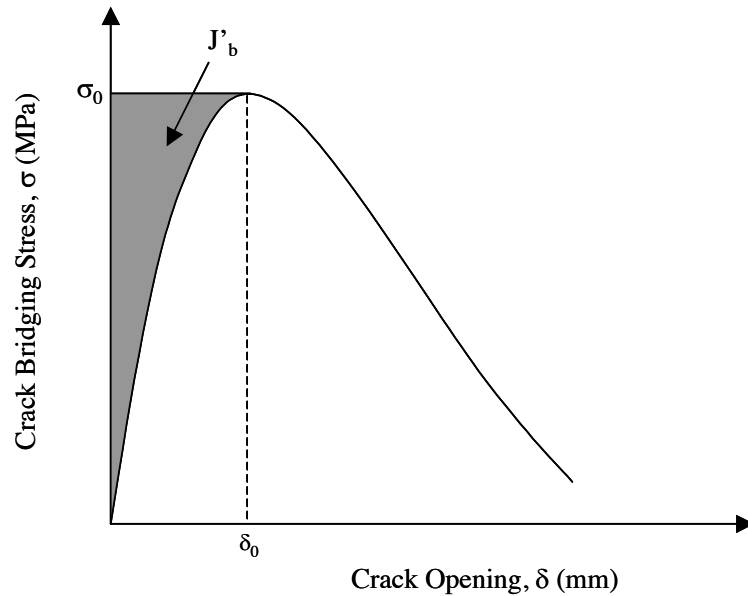


Figure 2.5 Crack bridging stress versus crack opening relation

where, σ_0 is the maximum crack bridging stress and σ_{fc} is the first cracking strength of the mortar matrix. For saturated multiple cracking, Wang and Li (2004) found that Equation-2.2 must be satisfied at each potential crack plane, where σ_{fc} is understood as the cracking stress on that crack plane.

Development of multiple steady state crack formation and strain hardening behavior can be well understood through the attainment of ECC mixture that adequately meets the two abovementioned parameters. However, along with the formation of steady state cracks, the material design must be made to obtain crack widths less than 100 μm threshold limit. This need can be satisfied with the tailoring of crack bridging versus crack opening relation stated in Equation-2.1. As shown in Figure 2.5, during the multiple microcracking of ECC material, the maximum steady state crack width can be regarded as δ_0 and the crack width accounting for the maximum crack bridging stress as σ_0 . Crack bridging stress starts to decrease, if crack width exceeds δ_0 value. In this case, localized cracks start to occur and the formation of multiple steady state microcracks ceases. However, as δ_0 value is kept under 100 μm threshold, multiple microcracking and strain hardening behavior can be acquired.

Lin et al. (1999) proposed the formulation of the crack bridging stress versus opening relationship based on summing the bridging force contribution of fibers that cross a given crack plane. This relation is expressed in Equation-2.3.

$$\sigma(\delta) = \frac{4V_f}{\pi d_f^2} \int_{\phi=0}^{\pi/2} \left(\int_{z=0}^{(L_f/2)\cos\phi} P(\delta) e^{f\phi} p(\phi) p(z) dz \right) d\phi \quad (2.3)$$

where V_f is the fiber volume fraction, d_f is the fiber diameter, ϕ is the orientation angle of the fiber, L_f is the fiber length, z is the centroidal distance of a fiber from the crack plane, f is a snubbing coefficient, and $p(\phi)$ and $p(z)$ are probability density functions of the fiber orientation angle and centroidal distance from the crack plane, respectively. $P(\delta)$ is the pullout load versus displacement relation of a single fiber aligned normal to the crack plane, also described in Lin et al. (1999). The factor $e^{f\phi}$ accounts for the changes in bridging force for fibers crossing at an inclined angle to the crack plane.

Through the use of basic micromechanical models, ECC material can be tailored to endure larger strains up to several percent without the formation of larger cracks that could cause an increase in overall permeability. The application of material design procedures, such as those outlined above, allow materials engineers to carefully match material characteristics to specific structural demands, such as strain capacity and low permeability.

2.4 Self-Healing Techniques in Cementitious Composites

Injured skins and tissues have ability to self-heal themselves since new healing materials are produced by the body itself and replaced with the damaged parts. Self-healing in cementitious composites is a process that is inspired from nature, human body and so on. Likewise, it is highly desirable in the case of cementitious composites to seal its own damage when cracking is observed. Therefore, during the past few decades many newly developed self-healing approaches have emerged. Some of these techniques were summarized in the following sections.

2.4.1 Microencapsulation

As in many other techniques, encapsulation was also inspired by the nature. The examples can be ranged related to this technique from an egg of bird which is macroscale to a human cell containing its own components which is nanoscale (Hemsley and Griffiths, 2000). Microencapsulation was first started to be developed with the production of capsules incorporating dyes which were mostly used for the replacement of carbon paper and copying purposes (Scheicher and Green, 1956). In time, encapsulation gained more and more popularity in many fields. Microencapsulation means of a technique in which a specific type of very small particles are inserted inside of a protective shell to isolate the specific materials from the external environment where they are subjected to. White et al. (2001) were one of the first to show the utilization of capsules containing healing agents for the self-healing purposes. The microencapsulation approached followed in this study was shown in Figure 2.6. As seen in the figure, with the occurrence of a crack, rupture comes into contact with the capsules leading to the release of self-healing agent near

the crack faces. The self-healing agent was drawn to near-crack faces through capillary action. When the self-healing agent contacts with the previously inserted catalyst, polymerization starts and the cracks are sealed. In another study undertaken by Boh and Sumiga (2008) microencapsulated additives were used during the production of building and construction materials with the purpose of increasing the hydration capability of the cementitious matrix. In another study, an epoxy resin having two different components one of which was used as a hardener and has a different capsule diameter were utilized to trigger self-healing through encapsulation (Nishiwaki, 1997).

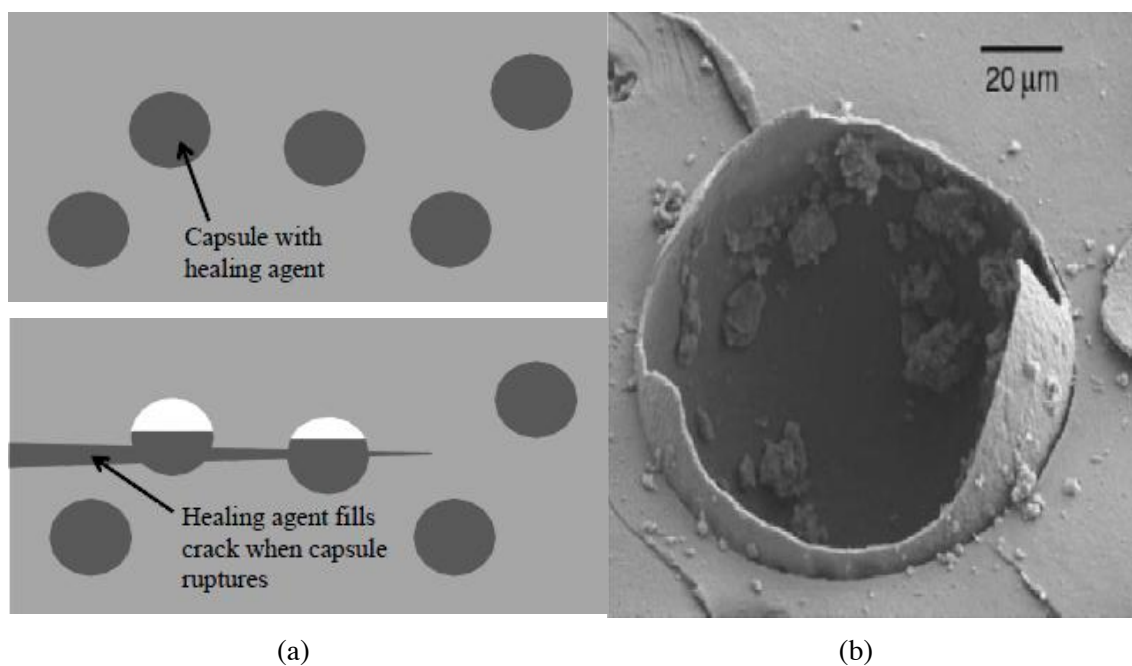


Figure 2.6 a) Basic method of the microcapsule approach (Li and Herbert, 2012) b) ESEM image showing a ruptured microcapsule (White et al., 2001)

In order to understand whether this technique is problematic or not some compression and splitting tests were performed and it was concluded that there are technical problems related to the quantity of healing agent to entirely fill the cracks, size of microcapsules and bonding strength between the matrix itself and microcapsules. Rattner (2011), investigated the sodium silicate incorporated microcapsules and their relation to self-healing capability. According to his research, after almost a week of curing period, nearly failed specimens were able to recover 26% of their original strength with the only 2% microencapsulation while healing in terms of strength recovery was only 10% in the case of control specimens.

2.4.2 Hollow Fibers

The utilization of hollow fibers inside of an engineering structure is actually inspired by the arteries in a human body. Hollow fibers which are also called as hollow pipettes or tubes depending on the diameter store the specific component or rather self-healing agent which would be freed in the incident of cracking.

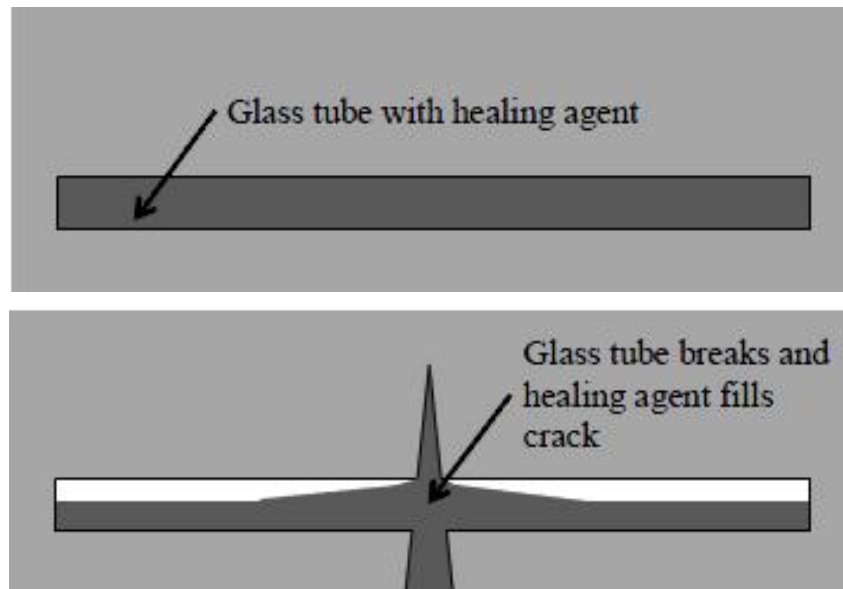


Figure 2.7 Schematic illustration of glass tubing self-healing approach (Li and Herbert, 2012)

It can be stated that utilization of hollow fibers can be accepted as a special type of encapsulation except with the fact that more healing agent can be carried with the fibers (capsules) compared to microencapsulation method. Chemical additives in a great variety were utilized by several researchers over the years. Such additives include methylmethacrylate (Dry and McMillan, 1996), ethyl cyanoacrylate (Li et al., 1998; Joseph et al., 2010), polyurethane combined with an accelerator (van Tittelboom et al., 2011) and so on. It has been reported in these studies that, concrete can heal its own damage in terms of both mechanical and transport properties with the use of hollow tubes filled with healing agents. Special care was given to choose chemical additives with low viscosity since it makes it easier for the additive to easily flow and fill the cracks.

Mihashi et al. (2000) also studied the influence of hollow fibers on self-healing capability of a cementitious matrix. In this study, one end of the fibers

wassealed while the other end was left open to air for further supply of healing agent. In Figure 2.8, the test set up used for this study was shown.

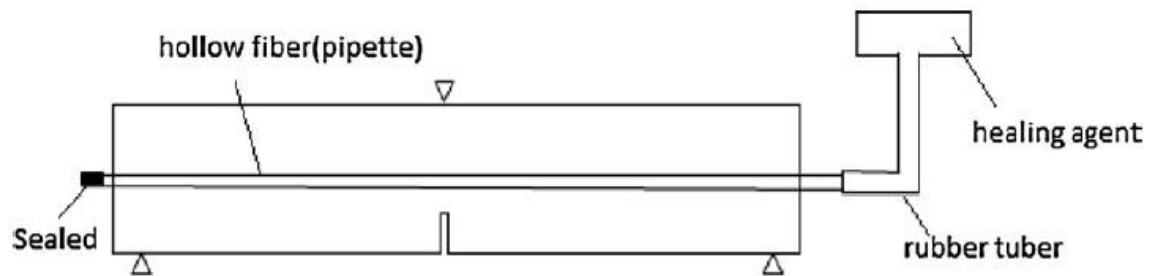


Figure 2.8 Schematic diagram of external healing agent supply system (Mihashi et al., 2000)

In the cited study, two different types diluted and non-diluted alkali-silica solution and an epoxy resin with two components having low viscosity were used as healing agents. Once the preparation was finished, specimens were pre-loaded until the crack mouth opening displacement which was between the values of 0.03 and 2.00 mm and then the load was released. With the completion of pre-loading, specimens cured until the next testing time. As a result it was observed that strength recovery ratios compared to the specimens with no healing agent was nearly 1.1 in the case of specimens incorporated diluted healing agent while this ratio was increased to 1.5 when non-diluted self-healing agent was incorporated. In the case of specimens incorporating epoxy resin as a healing agent, the strength recovery ratio was found to be rather low. The reason for lower strength improvements in the case of utilization of epoxy-filled hollow fibers was found to be in relation with inadequate mixing and stirring of the two components. According to the author, other reason for lower strength improvement was remaining of epoxy resin inside the tubes since one end was closed. In a similar study, Joseph et al. (2007) used the same testing equipment with small changes. The test set up used in this study was shown in Figure 2.9. In his study, Joseph et al. (2007) used ethyl cyanoacrylate as the healing agent. The conclusions drawn from this study showed that adequate self-healing is possible to attain when ethyl cyanoacrylate based healing agent supplied via an external supply system. It was shown that stiffness, peak load and ductility of the specimens were increased after the healing took place. Visual observations also suggested that under the influence of gravity and capillary suction ethyl cyanoacrylate was able to penetrate to a considerably large area.

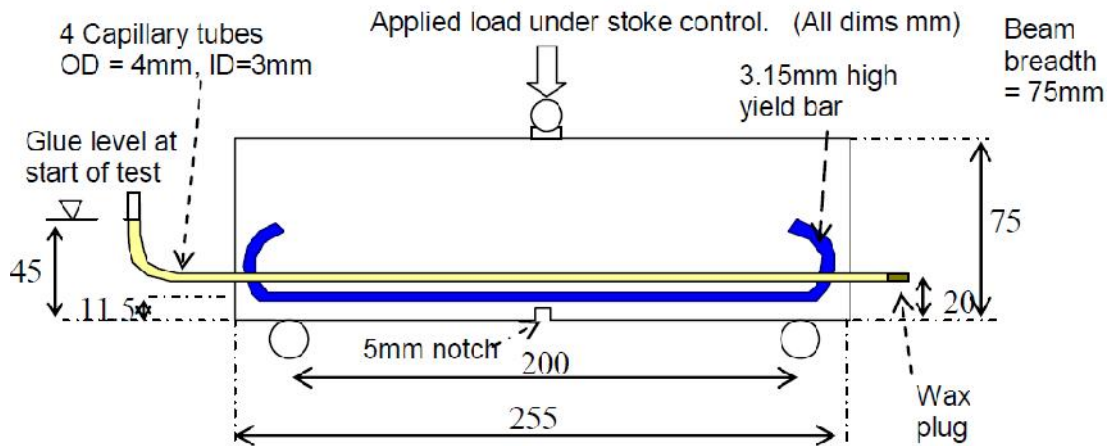


Figure 2.9 Experimental configuration used throughout the tests (Joseph et al., 2007)

Thao et al. (2009) conducted a study for the selection of optimum healing agent, carrier and container for the healing agent. In this study, epoxy resin with one component having a viscosity range of 250-500 cPa.s was preferred to be used as a healing agent. For the selection of tubes that will cover the healing agent, a comparison has been made between Perspex and glass tubes. It has been reported that the usage of glass tubes was more suitable since glass does not react with the epoxy resin and its brittleness makes it easier for healing agent to flow in the case of crack occurrence. When the dimensions were evaluated it was concluded that 4 mm and 6 mm are the optimum inner and outer diameters for the glass tubes, respectively.

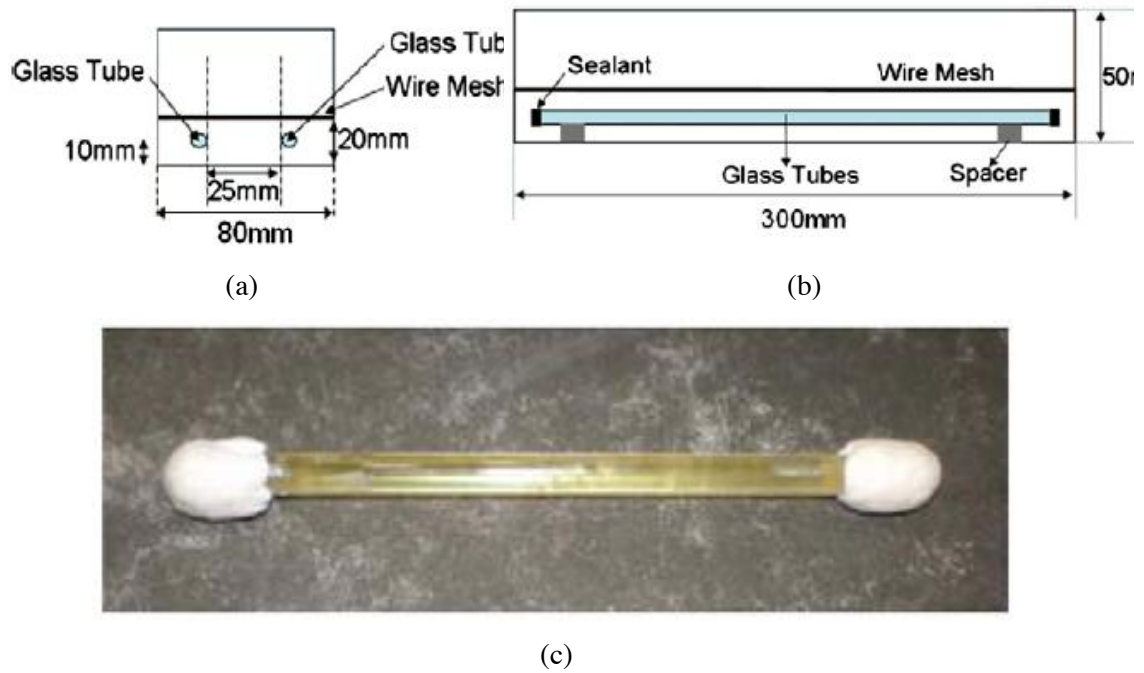


Figure 2.10 Self-healing system of internal encapsulation method with hollow glass tubes (a) middle section view (b) side view (c) epoxy-filled glass tube with a quastick as sealant (Thao et al., 2009)

After the several parameters that could affect the performance of self-healing capability were set, the experimental study was conducted to see whether the parameters are actually working. In Figure 2.10, test setup and specimens that were used throughout the tests were shown. During the cited study, firstly control specimens were failed in order to assess the load-displacement curves. Specimens having glass tubes were tested until the voice of fracturing was heard and the loading kept constant until the epoxy leakage was visually observed from the bottom surface of specimen. After 3 days of curing period, specimen was loaded until failure. It was concluded that the glass tubes chosen for this study was capable of easily fracturing in the incident of cracking which makes the release of self-healing agent easier. The utilized epoxy resin was proven to be flowable with the influence of gravity and capillary action. Some part of the strength of specimen was recovered after 4 days of healing. Moreover, in order to prevent the glass tubes from being broken with the influence of mixing, protection which is provided by 6.5 mm all-round mortar layer was recommended.

2.4.3 Bacteria Additive

In the case of bacteria addition to the cementitious matrix, self-healing capability was obtained through the calcium carbonate precipitation induced by the carbonation generation by the bacteria itself in an environment containing high levels of calcium. The mechanism for the self-healing supplied through bacteria addition was shown in Figure 2.11.

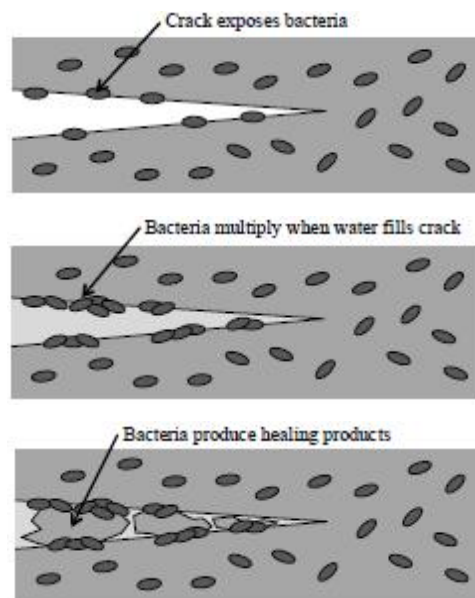
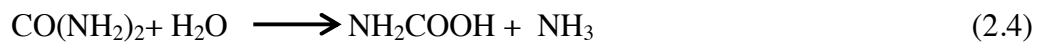


Figure 2.11 Schematic illustration of bacteria additive self-healing approach (Li and Herbert, 2012)

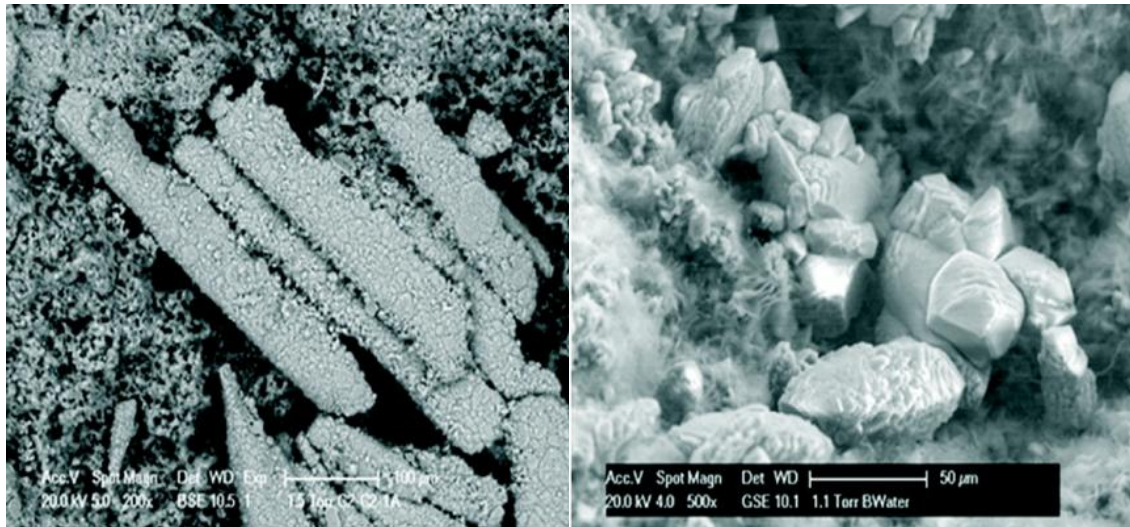
For this self-healing technique, the bacteria selection should be made very carefully so that it could withstand the highly alkaline cementitious environment and compressive pressures that would increase as the cement hydration improves at the later ages. Another important point is the availability of nutritious substances to feed the bacteria. Bacteria based self-healing was applied by several researchers (Jonkers et al., 2008; van Tittelboom et al., 2010). Gollapudi et al. (1995) were one of the first to apply biological repair technique for crack healing in concrete. In this study ureolytic bacteria were added to the concrete to help the precipitation of calcium carbonate (CaCO_3) in the near-microcrack places. The determination of microbial calcium carbonate precipitation was made by taking into consideration several parameters such as concentration of dissolved inorganic carbon, pH value, concentration of calcium ions, and the presence of nucleation sites. While the first three parameters were supplied by the metabolism of the bacteria, nucleation sites

where the reactions would take place were the cell walls of the bacteria (van Tittelboom et al., 2010).

In the study undertaken by vanTittelboom and coworkers (2010), a kind of bacteria that would produce urease enzyme which could actively participate in catalyzation of urea ($\text{CO}(\text{NH}_2)_2$) into ammonium (NH_4^+) and carbonate (CO_3^{2-}) were utilized. The chemical reactions that were involved were explained as follows:



As also seen from the reactions, first, 1 mole of urea is being hydrolyzed to 1 mole of carbamate and 1 mole of ammonia (Equation-2.4), then a spontaneous reaction takes place and carbamate hydrolyses to form 1 mole of ammonia and 1 mole of carbonic acid (Equation-2.5). After that, these products are used to form 1 mole of bicarbonate, 2 moles of ammonium and hydroxide ions as seen from Equation-2.6 and 2.7. Equation-2.6 and 2.7 cause the pH value to increase which leads bicarbonate equilibrium to be shifted and carbonate ions to be produced as seen from Equation-2.8 (van Tittelboom et al., 2010). The bacteria have cell walls that are negatively charged and these walls can easily attract positively charged ions from the environment and deposit them in their wall surface. Along these lines Ca^{2+} ions show reaction with CO_3^{2-} ions leading to the calcium carbonate formation. The formation of CaCO_3 which was explained in Equation 2.9 and 2.10 can serve as nucleation sites. In Figure 2.12, precipitated CaCO_3 particles over the cracks were shown in different shapes.



(a)

(b)

Figure 2.12 ESEM images showing self-healing activity through calcium carbonate formation with scale bars of a) 100 μm , b) 50 μm (Van der Zwaag, 2010)

Wiktor and Jonkers (2011) used encapsulated spores of calcium lactate based “*Bacillus pseudofirmus*” and yeast extract based “*Bacillus cohnii*” as bacteria. Bacteria were utilized in porous expanded clay particles having maximum size of 4 mm. It was concluded that after 100 days of submersion in water, calcium carbonate precipitation was visually observed near the crack faces showing the occurrence of self-healing. In the study performed by Wang et al. (2012) immobilized “*Bacillus sphaericus*” inside of silica gel and polyurethane used inside of glass tubes were utilized for the self-healing purposes. As a result it was observed that in the cases where there are high amounts of calcium ions are present in the environment, calcium carbonate precipitation was observed on the walls of bacterial cells which led to decreases in permeability coefficient and regains in some of the mechanical properties.

2.4.4 Mineral Admixtures and Expansive Agents

Mineral admixtures and expansive agents were used in some studies with the purpose of reducing the permeability of concrete after crack formation. The schematic representation of the proposed approach was shown in Figure 2.13.

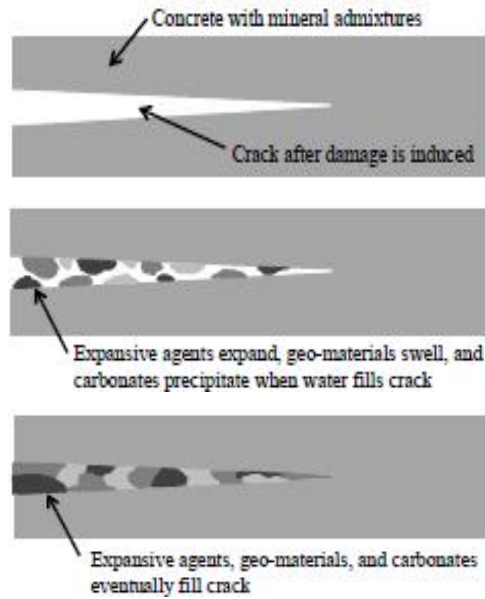


Figure 2.13 Schematic illustration of mineral admixture based self-healing approach (Li and Herbert, 2012)

Cementitious products obtained as a result of hydration reactions (AFt, AFm, CaCO_3 and CH) and the formation of these materials was observed in several studies (Kishi et al., 2007; Ahn, 2008). It was believed that some of the hydration products listed above is leached out and show crystallization in the water flowing through the cracks. Along these lines a new self-healing approach was tried to be developed by several researchers (Ahn and Kishi, 2010; Kishi et al., 2007; Ahn, 2008). In a study conducted by Kishi et al. (2007) performance comparison has been made between a reference concrete sample having no expansive agent and a concrete sample of whose 10% of cement was substituted with the combination of $\text{C}_4\text{A}_3\text{S}^-$, CaSO_4 and CaO . It was concluded from the experimental results that after one month of curing period of concrete beam specimens, cracks with the widths reaching nearly $220 \mu\text{m}$ levels were healed. The observed self-healing products were produced as a result of rehydration. In the case of normal concrete mixtures incorporating no expansive agents, the crack widths showed slight reductions during the same time period. In another study (Ahn and Kishi, 2008), changes in the self-healing capability was observed after adding an expansive agent in combination with a geo-material having SiO_2 content of 71.3% and Al_2O_3 content of 15.4%. As a conclusion drawn from this study, it was stated that individual aluminate and silicates which were dissolved from their original sources in the presence of alkali metals and high pH levels polymerized and resulted in the formation of geo-polymers. Additionally, it was concluded that size of the gels in geo-polymeric form was less than $2 \mu\text{m}$ level and near the cracking

zones there was several hydrogarnet phases formed. The formation of hydrogarnet or AFt phases which significantly affected the self-healing of cracks was also confirmed by visual observations as shown in Figure 2.14. In some of the studies referenced above, influence of chemical additives on self-healing capability was investigated as well (Ahn and Kishi, 2008; Ahn and Kishi; 2010). As a result of these studies, utilization of several carbonate species such as NaHCO_3 , Na_2CO_3 and Li_2CO_3 inside of conventional concrete mixtures was found to be beneficial in terms of recrystallization and particle precipitation. It was reported that through the usage of suitable carbonate dosages and expansive agent, crack healing capability could be improved.

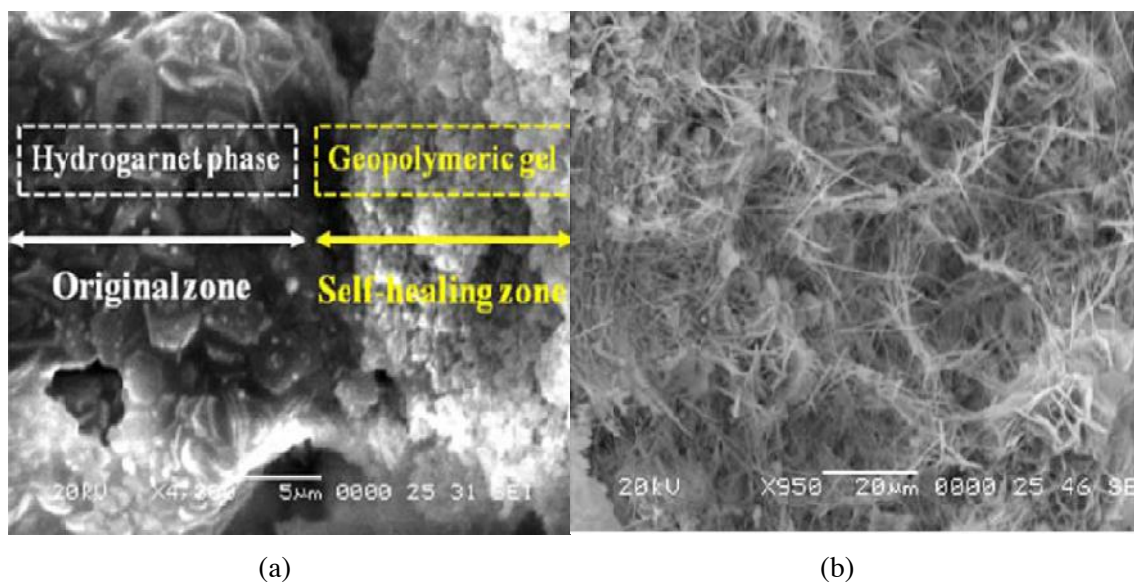


Figure 2.14 ESEM image of healing products. (a) Comparison between geopolymeric gel phase from self-healing area and hydrogarnet phase from original area (b) formation of hydrogarnet phases, AFt phases and calcite in self-healing zone (Ahn and Kishi, 2008)

2.5 Pozzolanic Material

According to ACI 116R-90 (1994), pozzolan is “a siliceous or siliceous and aluminous material, which in itself possesses little or no cementitious value but will, in finely divided form and in the presence of moisture, chemically react with calcium hydroxide at ordinary temperatures to form compounds possessing cementitious properties.” Mineral admixtures that are, or both cementitious and pozzolanic can be used as a partial replacement for Portland cement. Some of the most used materials are ground granulated blast furnace slag (slag hereafter), fly ash, condensed silica

fume. When properly used as a portion of the cementitious material, these pozzolanic admixtures can improve the properties of the fresh and hardened concrete.

Although several types of supplementary cementitious materials exist, the focus of this review will be on the two types used in this study, namely slag and fly ash. A brief overview of the history, properties, and usage of granulated blast furnace slag and fly ash in concrete is presented in Sections 2.5.1 and 2.5.2.

2.5.1 Slag

Slag has been used as partial replacement for Portland cement in concrete for more than 100 years (Glasser, 1991). As a by-product of the pig iron industry, slag is produced in large quantities in many areas around the world. In the United States, slag is most commonly used as base course for roads and other structures. However, in many other countries, most of the available slag is ground to approximately the same fineness as cement and then utilized as a partial replacement for Portland cement in concrete.

The composition of slag can vary considerably between production facilities. The presence of the major oxides are typically found to be within the following ranges: magnesium oxide (MgO), 0 to 21 %; aluminum oxide (Al₂O₃), 5 to 33 %; silicon dioxide (SiO₂), 27 to 42 %; and calcium oxide (CaO), 30 to 50 % (Taylor, 1997). Although the composition of slag is important, the method used in its production is perhaps more important as air-cooled slag has very limited, if any, cementing properties (Moranville-Regourd, 1998). However, if the slag is cooled rapidly from its liquid state at 1350-1550 °C down to about 800 °C, crystallization of the material can be avoided and the resulting product often contains over 95% glass which is a latent hydraulic cement (Taylor, 1997).

For any substantial reaction to occur between slag and water, an activator is required. High alkaline environments have proved to be suitable activators. Fortunately, the pore solution of cement paste is basically composed of alkaline hydroxides and as such, provides for an excellent activator. The use of slag in concrete tends to slow

down the rate of hydration at early ages at room temperature. However, elevated temperatures help activate the slag and increase the rate of hydration (Roy, 1992). Therefore, slag can be used in steam-cured concrete. In addition, the damaging effects, such as reduced strength and increased permeability, of high early age temperature on concretes containing slag are less pronounced than when slag is not used (Neville, 1996).

The reaction of a blend of cement and slag results in a higher percentage of calcium-silicate-hydrate (C-S-H) and less calcium hydroxide than plain cement (Neville, 1996). This alteration in the hydration products is attributable to the higher silicon content of the cement and slag blend when compared with plain cement. The change in the microstructure and the slower rate of hydration when slag is used typically yields denser and less permeable concretes.

In addition to lower permeability, concretes made with slag tend to have better resistance to chloride ion penetration than normal concretes. The freeze-thaw resistance of concrete made with slag is believed to be adequate and not adversely affected when compared with concrete made without slag (Neville, 1996). However, concretes made with slag generally suffer higher degree of deicing salt scaling than do reference concretes made without slag (Stark and Ludwig, 1997). Consequently, ACI Committee 318 (2002) limits the maximum amount of slag to 50 % of the total binder content if the concrete will be exposed to deicing chemicals. The total amount of slag and other supplementary cementitious materials is also limited to a maximum of 50 % of the total binder content.

2.5.2 FlyAsh

Fly ash is the most widely used mineral admixture for concrete. It is a byproduct of burning pulverized coal, in electric power production. During combustion, most of the volatile matter and carbon is burned off leaving the coal's mineral impurities (clay, feldspar, quartz, and shale) behind which then fuse together while in suspension. The fused particles are carried away by the exhaust by electrostatic precipitators or bag filters. During this process the fused material cools and solidifies

to form the spherical fly ash particles. Typical particle size is around 20 microns but may range from one micron up to as large as 100 microns. Surface area may range from 200-700 m²/kg but typically are between 300-500 m²/kg (Kosmatka and Panarese, 1988).

Fly ash consists primarily of silica, aluminum, iron, and calcium in a silicate glass form. Minor constituents can be found in the form of magnesium, sulfur, sodium, potassium, and carbon. According to American Society for Testing and Materials (ASTM), there are two classes of fly ash (Table 2.2): Class C, which is normally produced from lignite or subbituminous coals and Class F, which is normally produced from bituminous coals (ASTM C618, 2003). Class C fly ashes differ from Class F fly ashes in that they are self-hardening even without the presence of cement.

Table 2.2 Specifications for fly ash (ASTM C 618, 2003)

Class of Ash	ASTM Specification
Class C	SiO ₂ + Al ₂ O ₃ + Fe ₂ O ₃ > 50%
Class F	SiO ₂ + Al ₂ O ₃ + Fe ₂ O ₃ > 70%

CHAPTER 3

EXPERIMENTAL PROGRAM

3.1 Materials

3.1.1 Cement

The cement (PC) used in all mixtures was a normal portland cement CEM I 42.5R, which correspond to TS EN 197-1 CEM I type cement. It has a Blaine fineness of 460 m²/kg. Chemical composition and physical properties of cement are presented in Table 3.1.

Table 3.1 Chemical and physical properties of portland cement, fly ash and slag

Chemical Composition	PC	F	S
CaO	61.43	3.48	35.09
SiO ₂	20.77	60.78	37.55
Al ₂ O ₃	5.55	21.68	10.55
Fe ₂ O ₃	3.35	5.48	0.28
MgO	2.49	1.71	7.92
SO ₃	2.49	0.34	2.95
K ₂ O	0.77	1.95	1.07
Na ₂ O	0.19	0.74	0.24
Loss on Ignition	2.20	1.57	2.79
SiO ₂ +Al ₂ O ₃ +Fe ₂ O ₃	29.37	87.94	48.38
Physical Properties			
Specific Gravity	3.06	2.10	2.79
Blaine Fineness (m ² /kg)	325	269	425

3.1.2 Fly Ash

Class-F fly ash (F) conforming to (ASTM C618, 2003) requirements with a lime content of 3.48% obtained from Sugözü Thermal Power Plant was used. The chemical properties of FA are given in Table 3.1. The specific gravity and Blaine fineness of FA are 2.10 and 269 m²/kg, respectively. The particle size distribution of fly ash is provided in Figure 3.1. Figure 3.2 illustrates the particle morphology of the fly ash. The scanning electron microscope (SEM) image showed that the particles of fly ash had significantly smooth spherical particles in comparison to slag.

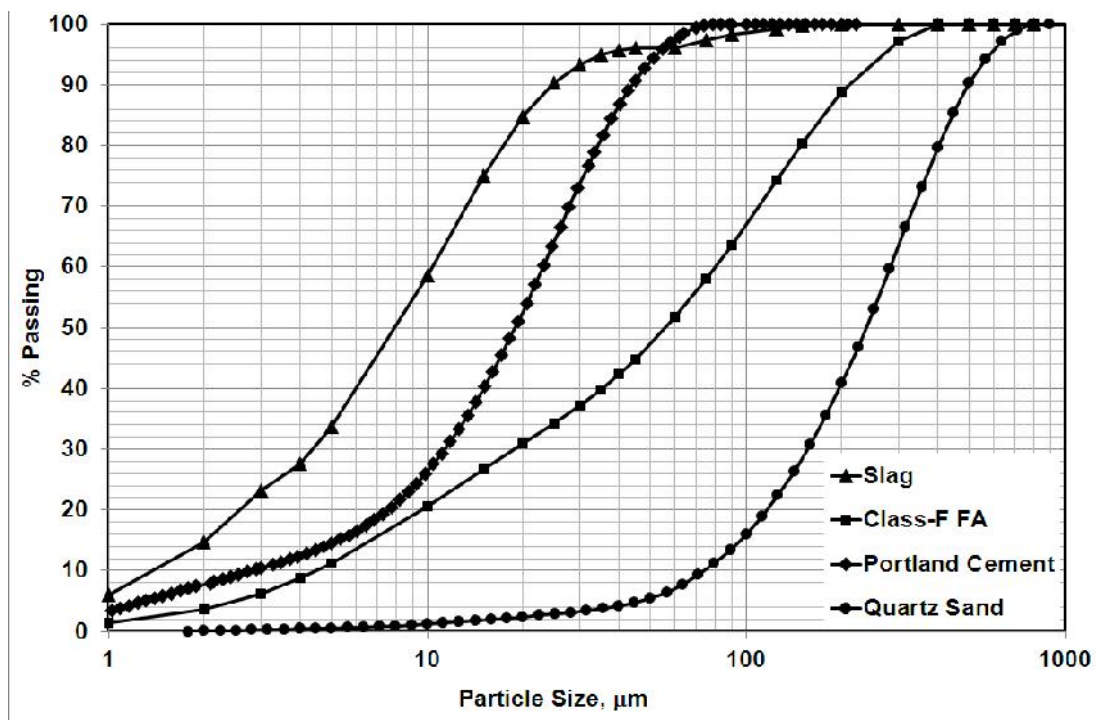


Figure 3.1 Particle size distributions of sand, portland cement, fly ash and slag

3.1.3 Slag

Slag (S) was supplied from Iskenderun Iron–Steel Factory in Turkey. Its chemical oxide composition is given in Table 3.1. The specific gravity of slag was 2.79 g/cm³. The slag was ground granulated in Iskenderun Cement Factory to have a Blaine specific surface area about 425 m²/kg. According to ASTM C989 (2009) hydraulic activity index, the slag used was classified as a category 80 slag. Particle size distribution of slag obtained by using the laser diffraction is shown in the Figure 3.1.

To identify morphological characteristics of slag, it was analyzed with SEM and the resulting photograph is presented in Figure 3.2.

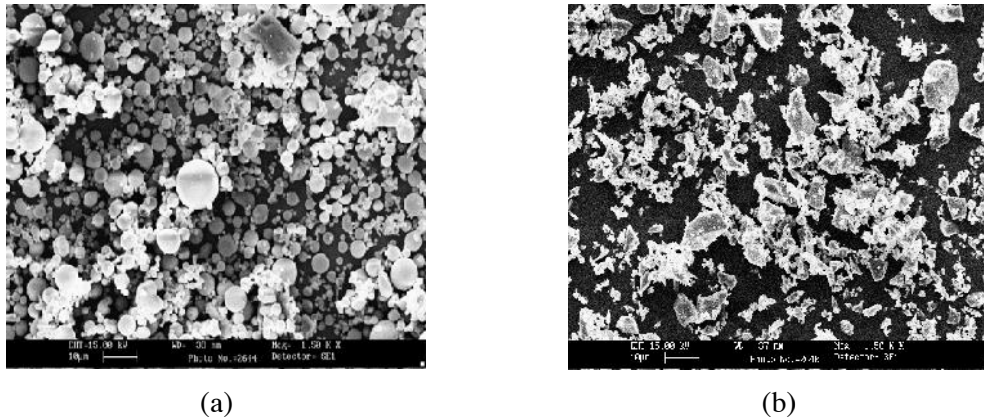


Figure 3.2 Particle morphology of a) Class-F fly ash b) slag determined by SEM

3.1.4 Aggregate

According to micromechanic-based design of ECC, exhibiting ductile and showing a large crack number, but small in width, of cementitious composites a low fracture toughness of the matrix is required. However, with the increasing of maximum grain size of aggregate, increase in toughness of the matrix is appeared and as a result, to obtain suitable ECC, aggregate grain size is limited (Li et al.,1995).



Figure 3.3A view of quartz sand aggregate

Therefore, so far, ECC has been produced successfully with an average grain size of about 110 μm (Li et al., 1995). Using high volumes of industrial by-product in the production of ECC decreases matrix fracture toughness and provides freedom of changing aggregate size. It is very important to produce ECC from normal size local sources of aggregate in terms of widespread application for both literature and our country. For this purpose, in the production of ECC, fine quartz (see Figure 3.3) with a nominal aggregate size (MAS) of 400 μm was obtained from local sources in Turkey's resources. Water absorption capacity and specific weight of quartz aggregate used is 0.3% and 2.60, respectively.

3.1.5 Chemical Admixtures

To improve the workability of ECC mixtures, Glenium 51, high range water reducing admixture (HRWRA – polycarboxylate ether as an active ingredient with 1.1 specific gravity and 40% solid content) produced by BASF Construction Chemicals was used.

3.1.6 Polyvinyl Alcohol (PVA) Fiber

Although different types of fibers have been utilized for the production ECC, PVA fiber was used in this study (Figure 3.4).



Figure 3.4 PVA Fiber used in the production of ECC

The use of PVA fiber was decided based on and PVA-ECC represents the most practical ECC used in the field (Li et al., 2001; Kunieda and Rokugo, 2006) at the present. PVA fibers have attracted most attention due to the outstanding composite performance and economics consideration. The dimensions of the PVA fiber are 8 mm in length and 39 μm in diameter. The nominal tensile strength of the fiber is 1620 MPa and the density of the fiber is 1300 kg/m^3 . The mechanical and geometric properties of PVA fibers are summarized in Table 3.2. The surface of PVA fibers were coated with hydrophobic oiling agent (1.2% by weight) for the purpose of reducing the interfacial bonding strength between fiber and matrix. To account for material inhomogeneity, a fiber content of 2% by volume in excess of the calculated critical fiber content has been typically used in the mix design. Decision on the usage of fiber was made according to ECCs micromechanical material design and it was experimentally proved that good properties are obtained as a result (Li et al., 2001; Kong et al., 2003).

Table 3.2 Mechanic and Geometric Properties of PVA Fibers

Fiber Type	Nominal Strength (MPa)	Apparent Strength (MPa)	Diameter (μm)	Length (mm)	Young Modulus (GPa)	Strain (%)	Specific Weight kg/m^3
PVA	1620	1092	39	8	42.8	6.0	1300

3.2 ECC Mixing and Specimen Preparation

Although self-healing of cement-based materials is of interest to many researchers, the availability of information related to the phenomenon especially in the case of multiple overloading conditions is rather lacking in the literature along with the dilemma of whether self-healing would take place in the entire structure or be limited to certain areas. In order to account for the related knowledge gap, an experimental study covering the influence of different SCMs and initial curing time on two robustness criteria of self-healing, repeatability and pervasiveness, was undertaken. With this purpose in mind, two different ECC mixtures incorporating Class-F fly ash (F_ECC) and ground granulated blast furnace slag (S_ECC) were prepared. Typical stress-deflection graphs of both mixtures obtained under four-point bending loading which exhibit superior deflection-hardening behavior of the specimens at the end of 28 days were provided in Figure 3.5.

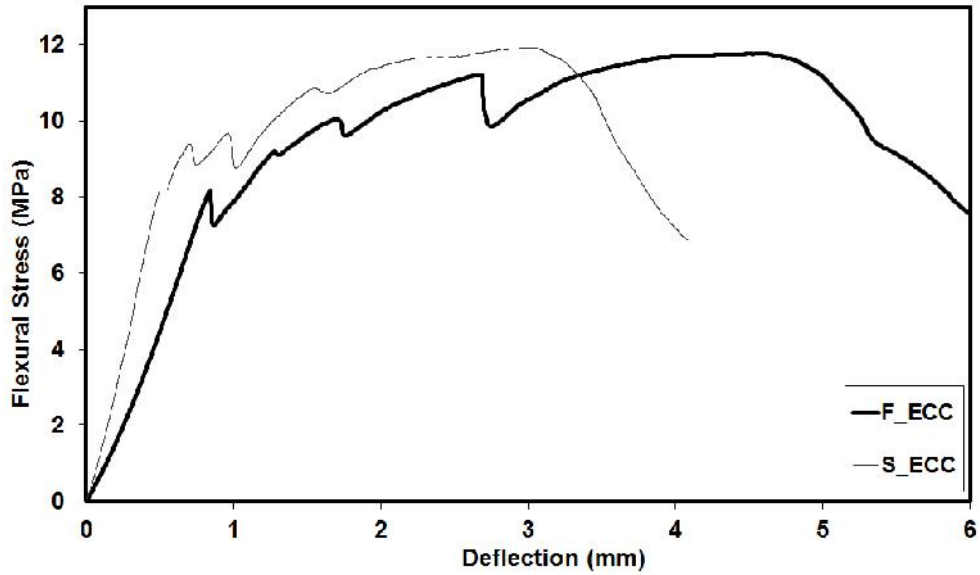


Figure 3.5 Typical flexural stress – mid-span deflection curves of ECC mixtures at age of 28 days

To produce mixtures with water to cementitious material ratio (W/CM) of 0.27 and mineral admixture (i.e fly ash [F] and slag [S]) to portland cement ratio (MA/PC) of 1.2, a gravity mixer was used. The details of mixture proportions were given in Table 3.3.

Table 3.3 ECC mixture proportions

Mix ID.	Ingredients, kg/m ³						MA/PC	W/CM
	PC	MA	Water	PVA	Sand	HRWRA		
F_ECC	566	680	331	26	453	5.1	1.2	0.27
S_ECC	593	712	347	26	474	6.0	1.2	0.27

To obtain approximately similar workability and uniform dispersion of fibers, the HRWRA content was varied from mix to mix. As seen from Table 3.3, the ECC mixture incorporating slag had higher HRWRA demand compared with the specimens casted with fly ash. It is likely to say that due to smooth surface characteristics and spherical shape of fly ash particles similar workability properties were obtained with lower HRWRA amount compared with slag particles at the same W/CM ratio (Figure 3.2).



Mixing of solid ingredients



Water addition



HRWRA addition



Fiber addition

Figure 3.6 Production of ECC by using Hobart Type mixer

In this study, a Hobart type mixer (Figure 3.6) with 20-liter capacity was used in preparing all ECC mixtures. Solid ingredients, including cement, mineral admixtures (F or S), and aggregate, were first mixed at 100 rpm for a minute. Water and HRWRA admixture were then added into the dry mixture and mixed at 150 rpm for one minute and then at 300 rpm for another two minutes to produce a consistent and uniform ECC matrix (without PVA fiber). PVA fiber was added at last and mixed at 150 rpm for an additional three minutes.

In order to determine self-healing capability in terms of repeatability and pervasiveness a series of cylindrical specimens with the dimensions of $\text{Ø}150 \times 300$ mm was cast to be used in resonant frequency (RF) tests. Specimens were demolded after 24 hours and cured in plastic bags at $95 \pm 5\%$ RH, $23 \pm 2^\circ\text{C}$ until the pre-determined testing ages. For rapid chloride permeability tests (RCPT), cylinder specimens measuring $\text{Ø}100 \times 200$ mm were produced and kept in plastic bags at $95 \pm 5\%$ RH, $23 \pm 2^\circ\text{C}$. At the age of 28 days, cylindrical specimens having dimensions of $\text{Ø}100 \times 50$ mm were extracted through the use of diamond blade saw and used in RCPT tests.

3.3 Pre-cracking and Self-Healing Evaluation Methods

As mentioned earlier, two test methods, RF and RCPT, were agreed upon to observe the changes in self-healing rates under repetitive pre-loading. To monitor the self-healing repeatability, transverse RF measurements based on ASTM C 215 were taken from $\text{Ø}150 \times 300$ mm cylinder specimens (ASTM C 215, 2008). Before being exposed to cyclic pre-loading, four 28-day-old $\text{Ø}150 \times 300$ mm cylinders from both mixtures were tested until failure under splitting tensile loading to define ultimate deformation capacities of different specimens (Figure 3.7). Ultimate splitting deformation capacities of specimens were found to be 2.1 mm and 1.9 mm for F_ECC and S_ECC mixtures, respectively. The actual tests were started after 3 and 28 days of initial curing and for each date, four cylindrical specimens were tested, one of which was kept as virgin (untouched) and the others were repeatedly pre-loaded up to 70% of their original deformation capacity under splitting tensile loading to achieve various amounts of microcracks. Pre-loading was applied in each 20 days up to 180 days for RF specimens. Between the time interval when each pre-loading was applied, specimens were subjected to wet-dry (W/D) cycles. W/D cycles consisted of the submersion of ECC specimens in water at $23 \pm 2^\circ\text{C}$ and drying in laboratory medium at $50 \pm 5\%$ RH, $23 \pm 2^\circ\text{C}$ for 24 hours. Since one W/D cycle takes two days, each 20 days-interval corresponds ten complete cycles. Additionally, changes in the widths of cracks formed over the specimens were observed with the help of portable microscope at the end of each ten cycle. In order to monitor whether the self-healing is restricted only in certain regions of the specimens or it is widely dispersive over the entire area, RF measurements were taken from two different

points, one at the top and the other in the middle, over $\text{Ø}150 \times 300$ mm-sized cylinder specimens.

Repeatability of self-healing was also monitored through RCPT tests. For RCPT, ten different 28-day-old cylindrical ECC specimens measuring $\text{Ø}100 \times 50$ mm were tested based on ASTM C 1202 procedure (ASTM C1202, 2002). Before the application of pre-loading, ultimate splitting deformation capacities of $\text{Ø}100 \times 50$ mm cylinder specimens after 28 days were found by taking the average results of four different specimens. The ultimate splitting deformation capacities of F_ECC and S_ECC specimens were 1.6 mm and 1.4 mm, respectively. By taking into consideration the final results, it was decided to keep four of the specimens as virgin and the rest to repeatedly pre-load up to 70% of their maximum splitting deformation capacity under splitting tensile loading. Pre-loaded specimens were then exposed to W/D cycles up to 100 days and in each 20 days RCPT measurements were recorded.

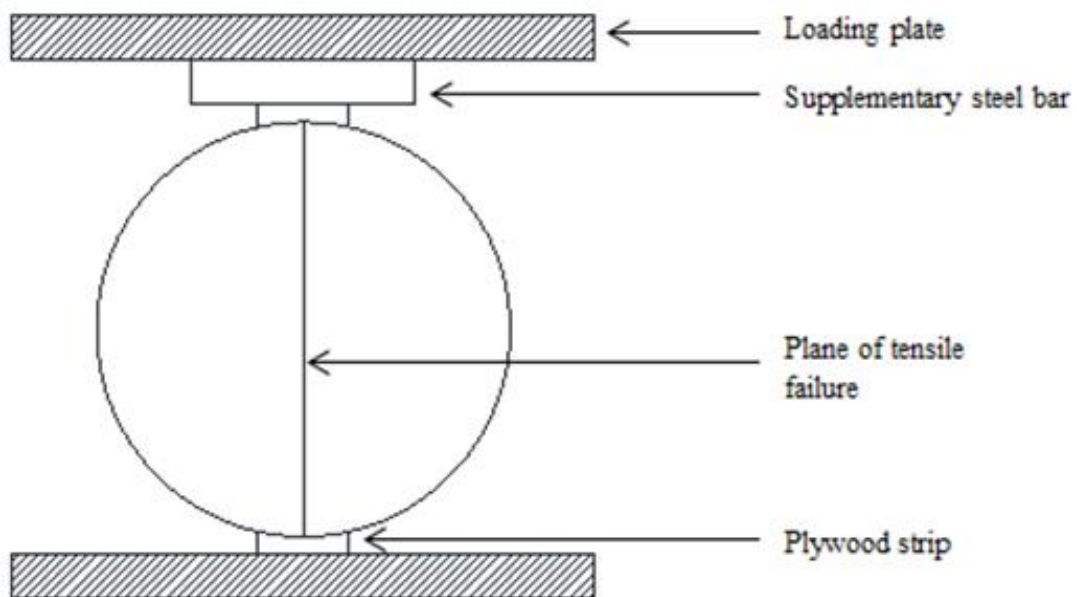
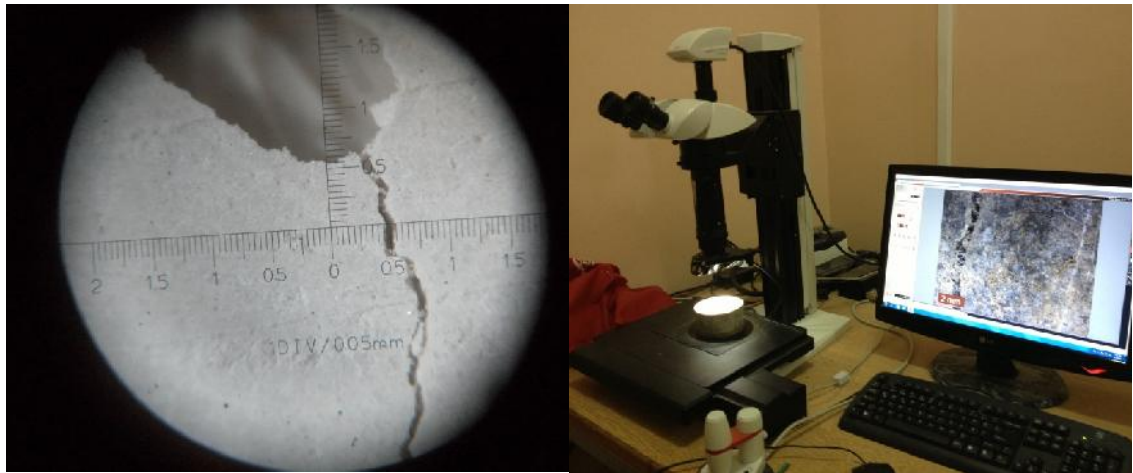


Figure 3.7 Splitting tensile strength test setup

At the end of each W/D cycle crack characteristics were analyzed from both faces in the case of RF cylindrical specimens. To do this a portable microscope was used (Figure 3.8). For cylindrical specimens used for RCPT tests an optical microscope with the maximum enlargement of 125X was used.



(a)

(b)

Figure 3.8 Observation of cracks under a) portable microscope b) video microscope

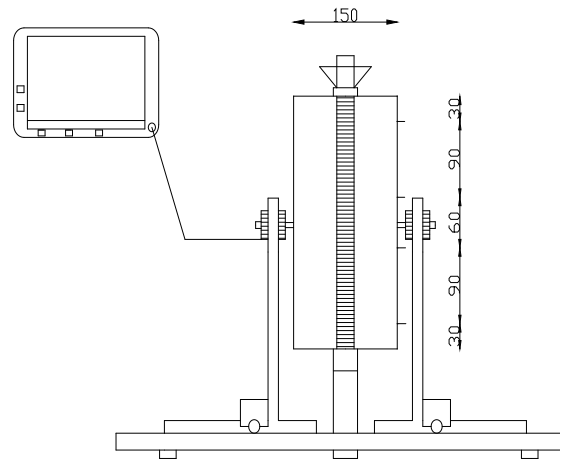
3.4 Test Procedure

3.4.1 Resonant Frequency (RF)

As previously mentioned resonant frequency tests were performed by using $\text{Ø}150 \times 300$ mm cylinder specimens in compliance with ASTM C215 (2008). The transvers RF measurements were assessed by means of a resonant based method in which an Erudite MK3 test device of working frequency range 1 Hz to 100 kHz, with EMAT vibrator and piezoelectric receiver (Figure 3.9). The device possesses both sonic and ultrasonic frequency ranges but the fundamental resonances obtained throughout the tests were in the sonic range because of the lateral specimen dimensions. As it can be seen from Figure 3.9, there are three different support conditions (two at the ends and one in the center point) where the specimens were placed. This was done to create fundamental resonance mode in the specimens more easily. The device works in a way that it changes the emission frequency of the pulse automatically until the maximum amplitude is obtained which implies the resonance of the wave in a specific specimen. The resonant frequency measurements were taken from top and middle portions of the cylindrical specimens and the results were averaged. From a certain point several readings were taken all in the direction of smallest length of the specimen which is 150 mm.



(a)



(b)

Figure 3.9a) View of resonant frequency test (RF) set up b) schematic representation of resonant frequency test setup

3.4.2 Rapid Chloride Permeability Test (RCPT)

Rapid chloride permeability test (RCPT) was performed by monitoring the amount of electrical current that passed through a sample 50 mm thick by 100 mm in diameter in 6 hours, which standardized with ASTM C 1202 (2002). This sample was cut as a slice of a 100x200 mm cylinder. A voltage of 60V DC was maintained across the ends of the sample throughout the test. One lead was immersed in a 3.0% salt (NaCl) solution and the other in a 0.3 M sodium hydroxide (NaOH) solution. Based on the charge that passed through the sample, a qualitative rating was made of the concrete's permeability (Figure 3.10).

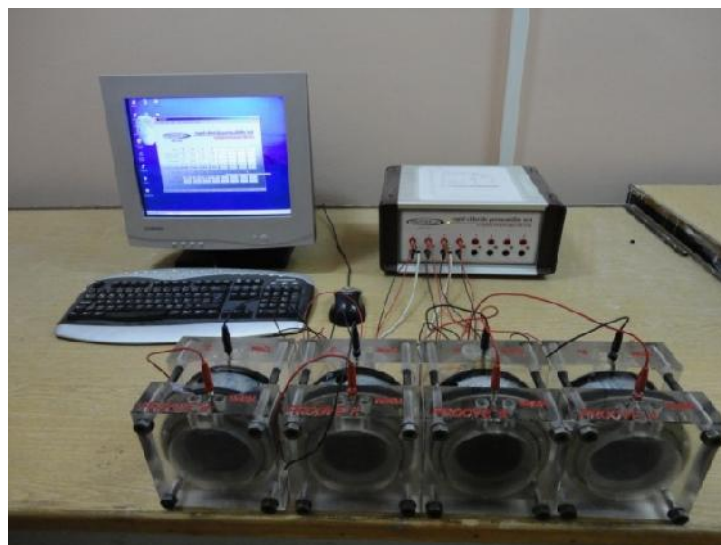


Figure 3.10 Rapid chloride permeability test (RCPT) setup

CHAPTER 4

RESULTS AND DISCUSSIONS

4.1 Resonant Frequency (RF) Test

4.1.1 Unhealed Specimens

Resonant frequency (RF) test results of ECC mixtures are presented in Figure 4.1. In the figure, measurements taken from the top and middle portions of 3 and 28-day-old virgin and pre-loaded ECC specimens were illustrated. Figure 4.1 was formed by using the initial RF measurements and percent variations observed according to the initial measurements beyond 3 and 28 days until the end of 90 W/D cycles. When both figures are carefully examined, it can be clearly seen that the RF results varied greatly depending on the changes in initial curing period, SCM types and number of W/D cycles. Original RF values obtained from top and middle portions of the 3-day-old F_ECC specimens were 1870 and 1515 Hz, respectively. In the case of 28-day-old F_ECC specimens the same values were 2050 and 2000 Hz. Original RF values recorded from 3-day-old S_ECC specimens were 1925 and 1695 Hz for the measurements taken from top and middle portion of the specimens, respectively. The same values were 2070 and 2000 Hz in the case of 28-day-old S_ECC specimens. As seen from Figure 4.1, an increasing trend in RF results was monitored for 3-day-old virgin specimens up to the end of 90 W/D cycles irrespective of the point where RF reading was taken and the type of SCMs used. The increase in RF results was fairly similar for both F_ECC and S_ECC mixtures. For example, at the end of 90 W/D cycles for 3-day-old virgin specimens, increment in RF results reached up to 146% and 140% of the initial readings for measurements taken from the top portion of F_ECC and S_ECC specimens, respectively. Same modality held true for readings taken from the middle portion of the specimens with the values reaching 129% and 121% for the same mixtures. Although, the final RF results of 3-day-old virgin ECC specimens incorporating FA and slag are found to be close to each other, F_ECC specimens showed slightly better performance than S_ECC specimens in terms of

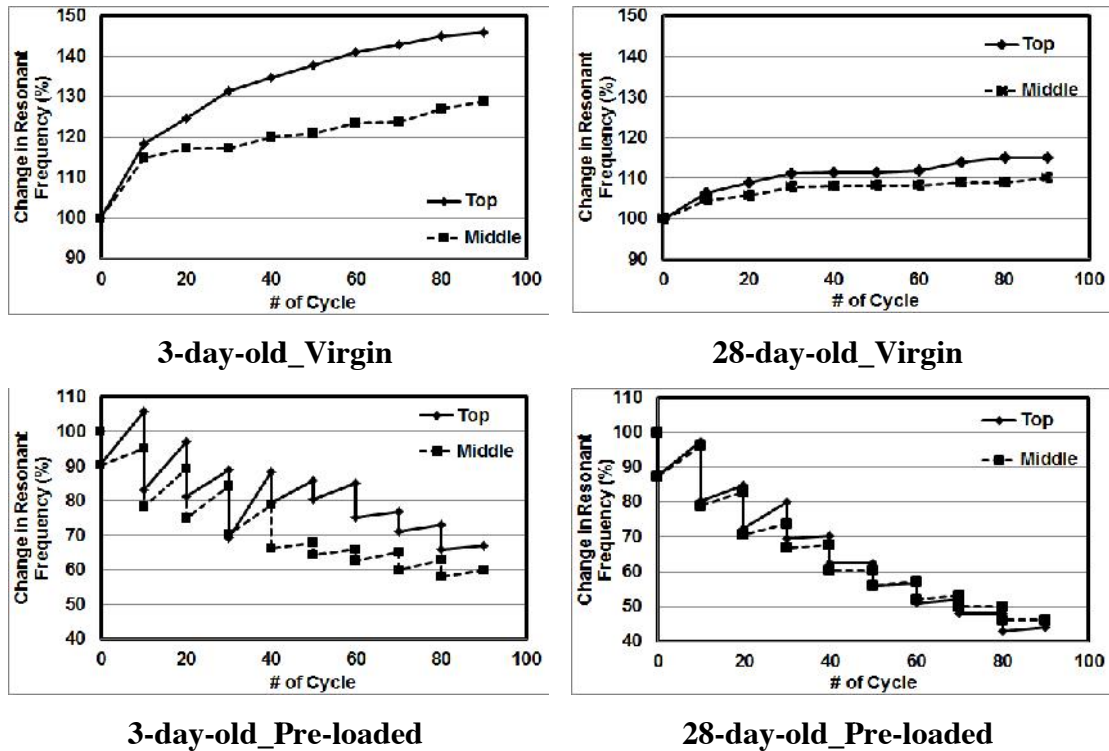
changes in RF measurements. The probable reason for this behavior of F_ECC specimens can be in relation with pozzolanic reactions, which could result in higher improvements in RF results compared with S_ECC specimens. This, therefore, implies that there is higher probability of F_ECC specimens to consume higher amounts of calcium hydroxide available in hydrated matrix especially in the late ages which could lead to higher improvements in RF measurements compared to S_ECC specimens.

The difference in RF results has become less pronounced for virgin specimens initially cured for 28 days. As seen from Figure 4.1, after 90 W/D cycles, 28-day-old specimens from both mixtures could exceed only 15% and 11% of the initial RF results for the readings taken from the top and middle portions of specimens, respectively. It was also obvious from the same figure that 20 W/D cycles were almost adequate for complete stabilization of the results in the case of 28-day-old ECC specimens. The reason for these specimens to show lower enhancement in RF with the increase in initial curing time could be related to the lower amounts of SCMs readily available in the systems to participate in further hydration reactions and reductions in pore sizes, densification of matrices and consequently lower overall transport of moisture, which is necessary for further hydration.

Another point worth mentioning in the case of virgin specimens is that without any regard to initial curing time and the type of SCM used, the RF measurements taken from the top portion of the specimens are found to be higher than the measurements taken from middle portion at the end of any number of W/D cycles. This behavior was continually observed from nearly all of the specimens so that the overall coefficient of variation was found to be less than 7% showing the consistency of results. This is most probably attributable to the changes in internal relative humidity of ECC specimens at different regions. According to Jiang et al. (2006) for cement pastes having W/CM ratio of higher than 0.40, moisture diffusion is the only mechanism leading to the reduction in internal relative humidity while moisture diffusion and self-desiccation caused due to chemical shrinkage of the paste have simultaneous influence on the reduction of internal relative humidity in the case of pastes with W/CM ratio of less than 0.40. Therefore, for ECC specimens with W/CM ratio of 0.27, it can be stated that during the W/D cycles, the diffusion of moisture to the short distances (points where the top and bottom RF measurements are taken)

was faster compared to longer distances (points where the middle RF measurements are taken).

F_ECC



S_ECC

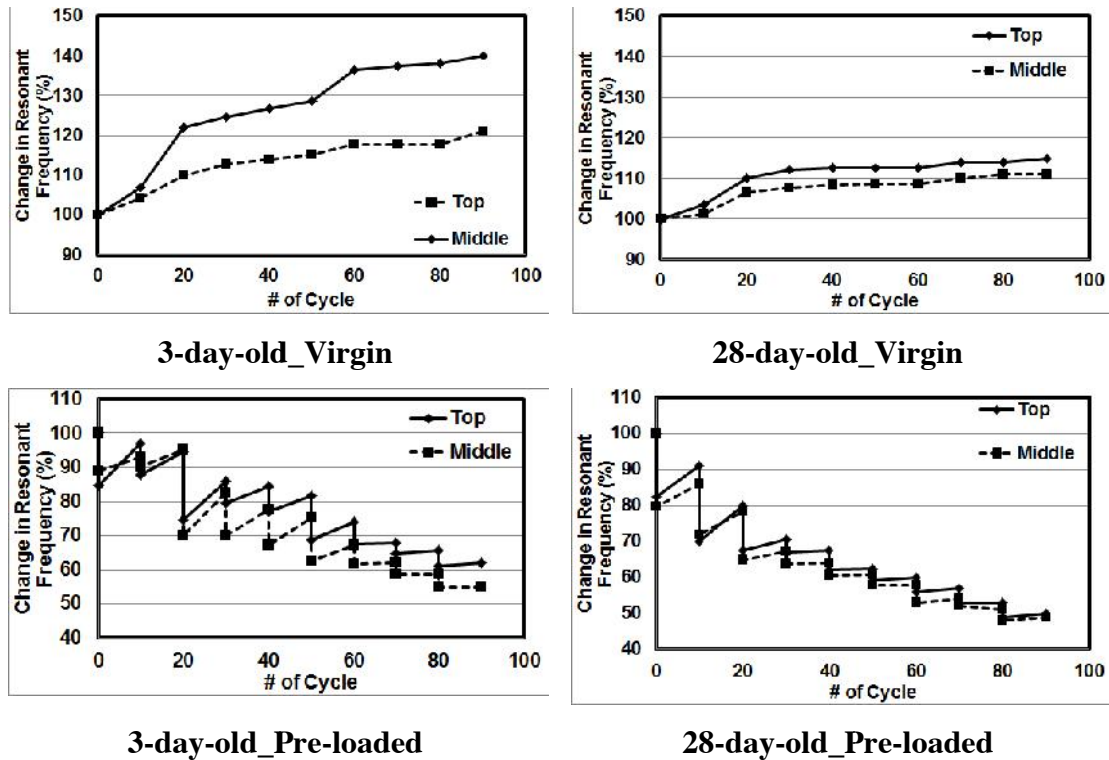


Figure 4.1 Percent variations in RF measurements due to repetitive pre-loading and subsequent conditioning

This led hydration kinetics to be faster and self-desiccation to be counteracted more easily at the top and bottom portion of specimens, which consequently brought along higher RF measurements to be obtained at the end of specified testing cycles.

4.1.2 Effects of Self-Healing

Percent changes in RF measurements taken from different ECC specimens which were repeatedly pre-loaded up to 70% of their maximum deformation capacities under splitting tensile loading at the end of each 10 W/D cycles until the completion of 90 W/D cycles, were shown in Figure 4.1. From each mixture, three separate specimens that were initially cured for 3 and 28 days were used to account for the likelihood of specimens to exhibit cracks in varying numbers and widths at the end of each pre-load applications, and the averaged results were used to construct Figure 4.1. As it is clear from the figure, with the application of pre-loading and exposure to different number of W/D cycles, the results showed fluctuations with varying rates. After each pre-loading applied at the end of each 10 W/D cycles, some reduction in RF results was monitored. The recovery of results which reflects the self-healing effect considerably changed depending on SCM type, number of W/D cycles and initial curing time. As it can generally be seen from Figure 4.1, the decrease in RF measurements with the application of pre-loading showed significant recovery at the end of different numbers of W/D cycles although this trend was found not to be everlasting. When the RF measurements taken from top portion of 3-day-old ECC specimens are carefully analyzed, it can generally be stated that increase in RF results started to level off after 60 W/D cycles for both ECC mixtures. The most probable reason for RF measurements to come to equilibrium after 60 W/D cycles is the excessive widening of cracks upon pre-load repetitions and gradual exhaustion of unhydrated cementitious materials in late age to account for the crack closure through self-healing. However, one should bear in mind that despite the stabilization of RF results beyond a certain time period, after the application of pre-loading to the specimens for six times, average RF results became only 85% and 74% of the initial RF measurement for F_ECC and S_ECC mixtures, respectively. This, therefore, shows that ECC materials produced in this study perform significantly well in terms of RF recovery under certain conditions implying the occurrence of self-healing

which could substantially decrease the repetitive repair and/or maintenance need. As stated above, the recovery of RF results just before the stabilization was found to be higher for F_ECC (85%) specimens compared to S_ECC specimens (74%) and this tendency of 3-day-old F_ECC specimens was observed to be true for each RF measurement taken after each 10 W/D cycles. This can be attributable to the changes in matrix composition of ECC specimens. As previously mentioned, Class-F fly ash used in this study contains more SiO₂ which is of importance for pozzolanic activity especially at later ages, while slag contains higher amounts of CaO which is mostly responsible of self-cementing behavior. Therefore, it is likely to say that S_ECC specimens performed their cementing reactions earlier than F_ECC specimens and this led faster consumption of unhydrated cementitious materials in the case of S_ECC mixtures. Instead, owing to the abundance of unhydrated fly ash particles even at later ages, F_ECC specimens showed higher improvements in RF measurements after each pre-loading and subsequent W/D cycles. According to Sahmaran et al. (2012), ECC specimens incorporating fly ash exhibit significantly tighter crack widths than specimens with slag due to increased limitations in matrix fracture toughness values. Thus, another reason for higher improvements of RF results in the case F_ECC specimens could be attributed to the reduced crack widths occurring with the application of cyclic pre-loading (see the section of “Crack Characteristics”).

It is clear from Figure 4.1 that the repeatability of self-healing in terms of RF measurements decreased significantly in the case of specimens initially cured for 28 days. As seen from the figure, the recovery results of both ECC mixtures showed stabilization after 30 W/D cycles with no regard to the point of measurement. The average recoveries obtained from top portion were found to be 80% and 71% of the initial RF measurements for 28-day-old F_ECC and S_ECC specimens after three pre-load repetitions, and 30 W/D cycles beyond which relatively small or no further RF recovery were monitored. The explanation for 28-day-old ECC specimens to exhibit stabilization in RF recovery results after 30 W/D cycles could be that due to increased initial curing time, the matrix maturity of specimens enhanced significantly leading to less unhydrated cementitious materials to be available in the systems for further hydration reactions to prompt self-healing behavior. Moreover, due to the continuity of hydration reactions matrix gets more compact at later ages which leads

to an increase in matrix/fiber frictional bond strength and fracture toughness values. Increments in these parameters are found to be detrimental for the attainment of sufficient multiple microcracking and could trigger localized crack formations with wider widths which may negatively influence crack closure through self-healing at later ages (Sahmaran et al., 2012).

As it was previously mentioned, two RF measurements were taken from surface and middle portion of ECC specimens. The motivation behind this was to better understand whether the self-healing of cracks is limited to the certain regions of specimens or rather dispersive over the entire area in the case of repeated pre-load applications and subsequent W/D conditioning. Generally speaking, the recovery of RF measurement taken from the middle portion of specimens were found to be lower compared to the recovery rates observed from surface portions (Figure 4.1). This behavior of specimens was more explicit for 3-day-old F_ECC and to a lesser extend for 3-day-old S_ECC mixtures. When the results from both surface and middle portions of 3-day-old mixtures are compared, it can be said that number of recovered pre-load repetitions before the stabilization of results did not change although the extent of recovery decreased in the case of measurements taken from the middle portions regardless of the mixture type. For example, by considering the surface portion measurements, after the application of six repetitive pre-loading while 85% and 74% of recovery observed in RF results for F_ECC and S_ECC mixtures, respectively, the values were 66% and 67% for the same mixtures in the case of measurements taken from middle portion. The same modality was true for 28-day-old specimens except with the fact that number of recovered pre-load repetitions before the stabilization of RF results decreased. In the case of 28-day-old specimens, after three repetitive pre-load applications, RF results taken from surface portion of specimens started to stabilize at 80% and 71% levels for F_ECC and S_ECC mixtures, respectively, while for results from middle portions after three pre-load applications recovery rates reached to 71% and 67% levels for the same mixtures. It can be deduced from these observations that near-surface cracks or rather cracks that could be more easily exposed to water can be healed up to 85% even after six times of severe deformation exposure due to easiness of moisture transport to shorter distances.

4.2 Rapid Chloride Permeability Test (RCPT)

4.2.1 Unhealed Specimens

Chloride ion permeability test results of cylindrical ($\text{Ø}100 \times 50$ mm) virgin ECC specimens were tabulated in Table 4.1. Each data presented in Table 4.1 was obtained by taking average of at least four different specimens.

Table 4.1 Rapid chloride permeability test results of ECC specimens

Mix ID.		0 cycles		0+10 cycles		0+20 cycles		0+30 cycles		0+40 cycles		0+50 cycles	
		Zero	AP*	BP [†]	AP	BP	AP	BP	AP	BP	AP	BP	AP
F_ECC	Virgin	3388	3388	1623	1623	1095	1095	775	775	548	548	347	347
	Pre-loaded	3349	4112	2291	3374	1878	2656	1782	2158	1736	2126	1798	2131
S_ECC	Virgin	995	995	759	759	662	662	497	497	465	465	441	441
	Pre-loaded	1064	1583	1160	1547	1302	1618	1409	1733	1639	1956	1885	2087

*: After pre-loading

†: Before pre-loading

The results were expressed in terms of total electrical charge in Coulomb which reflects the ECC materials' ability to resist chloride ion ingress. RCPTs were started after 28 days of initial curing since different SCMs show varying characteristics and low paste maturity restricts the implementation of the test by resulting in relatively high results.

According to the results obtained from virgin specimens (Table 4.1), it is clear that 50 W/D cycles caused marked reductions in RCPT results regardless of SCM type used in ECC specimens. Until the end of 50 W/D cycles, the results showed decreasing trend between 3388-347 and 995-441 Coulombs in the case of F_ECC and S_ECC mixtures, respectively. Another point that is visible at the first glance is that the drop in chloride ion penetrability results of F_ECC specimens was always higher than S_ECC specimens. This behavior of F_ECC specimens is more noticeable from Figure 4.2 which shows the percent changes in chloride ion permeability results with respect to the first measurement taken after 28 days of initial curing versus number of W/D cycles.

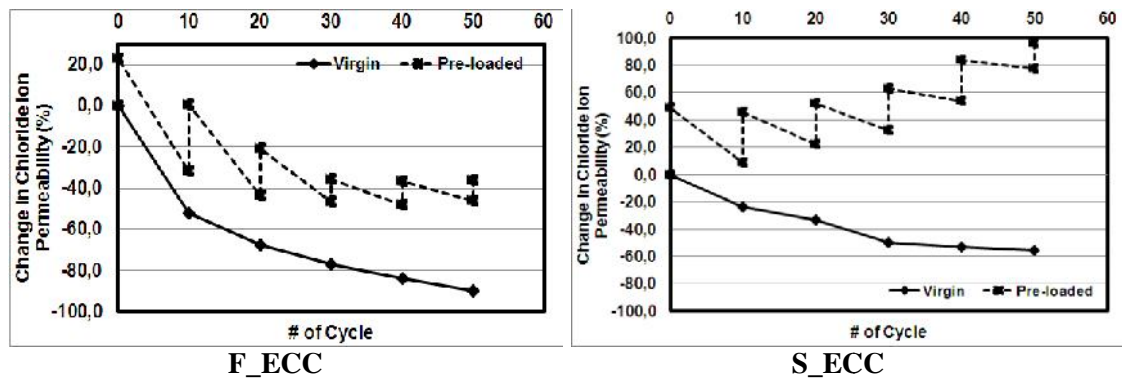


Figure 4.2 Percent variations in chloride ion permeability values of ECC mixtures due to repetitive pre-loading and subsequent conditioning

As seen from this figure, the reduction in chloride ion charge - number of cycle slope was found to be more explicit for F_ECC specimens compared to S_ECC specimens especially after the first 10 W/D cycles. For example, at the end of 10 W/D cycles, average chloride ion penetrability results of F_ECC specimens dropped by 52% while this value was 24% for S_ECC specimens. As the number of W/D cycles increases, the chloride ion charge - number of cycle slope started to be smoother for both ECC mixtures due to gradual diminishment of unhydrated cementitious materials with time. The probable reason for F_ECC virgin specimens to exhibit notable improvement in chloride ion penetrability results compared to S_ECC specimens can be closely related with the availability of unhydrated cementitious particles in greater quantities in matrices. This behavior of F_ECC specimens can also be evidenced by the fact that fly ash particles (especially Class-F fly ash) remain untouched in the system up to 30-40% without any chemical process leading to retardation of further hydration reactions (Song and van Zijl, 2004). Although, the improvement in final values was observed to be more pronounced for F_ECC specimen at the end of each W/D cycle, the chloride ion penetrability of S_ECC specimens were lower than the results obtained from F_ECC specimens after any number of W/D cycle excluding those obtained after 50 W/D cycles. The reason for S_ECC specimens to show lower RCPT results in comparison to F_ECC specimens may be associated with smaller particle size and higher cementing behavior of slag particles. As it is seen from Table 3.1, slag (425 m²/kg) is significantly finer than Class-F fly ash (269 m²/kg). Therefore, it can be deduced from here that the microstructure of S_ECC specimens became more compact due to enhanced filler

effect and higher cementing capability of finer slag particles especially during the early stages of hydration. Since RCPT is an electrochemical test method to be used for the evaluation of chloride ion permeability, the electrical conductivity of pore solution should also be accounted for during the assessment of results. Electrical conductivity of pore solution which can be critical for chloride ion penetrability test results can be reduced significantly by lowering the concentration of alkali ions (Na^+ and K^+) and associated hydroxyl ions (OH^-) (Shehata et al., 1999). Thus, lower alkali content of slag particles might also be a reasonable explanation for reduced RCPT results of S_ECC specimens (see Table 3.1). It must be emphasized that although the rate of improvement in RCPT results was lower for virgin S_ECC mixtures, even without the application of further W/D cycles, average chloride ion permeability test results of virgin S_ECC specimens was under 1000 Coulomb (995 Coulomb) which is regarded as the maximum value by ASTM C 1202 in order to call a certain material as very highly resistant to chloride ion ingress while virgin F_ECC specimens could reach to this level after 30 W/D cycles.

4.2.2 Effects of Self-Healing

Raw RCPT results of repeatedly pre-loaded cylindrical ($\text{Ø}100 \times 50$ mm) specimens were presented in Table 4.1 Each data given in the table was obtained by taking average of at least six different specimens. As seen from Table 4.1, with the application of repetitive pre-loading and cyclic W/D curing regime, results varied significantly. It is visible from Figure 4.2 that both of the ECC mixtures showed self-healing with a decreasing rate in terms of chloride ion penetrability results after each W/D cycles. The rate of self-healing for F_ECC specimens however was found to be higher than S_ECC specimens especially during the early ages. For instance, while F_ECC specimens showed 44% decrease in RCPT results after 10 W/D cycles, the same value was found to be 27% for S_ECC specimens. This behavior of F_ECC specimens was observed to be true throughout the entire W/D cyclic exposure however the difference between the healing rates of both ECC mixtures started to be less explicit due to lacking of unhydrated cementitious particles with time. Although it is less prominent in the case of F_ECC specimens, the healing rate of both mixtures decreased significantly beyond 30 W/D cycles. This finding is also in line

with what is stated in previous sections about the RF measurements taken from specimens initially cured for 28 days.

Another striking point is that application of five repetitive pre-loading and successive 50 W/D cycles in total led the average RCPT results of F_ECC specimens to decrease from 3349 to 1798 Coulomb and S_ECC specimens to increase from 1064 to 1885 Coulomb levels, respectively (Table 4.1). In other words, while the chloride ion penetrability test results of S_ECC specimens increased up to 77% of the initial reading after five pre-load applications and corresponding W/D cycles, the same result of F_ECC specimens decreased by 46% (Figure 4.2). This is interesting in that although comparable self-healing took place in both mixtures, after each pre-loading and corresponding cyclic W/D curing, the RCPT results of F_ECC specimens showed decreasing trend with respect to the first result taken at the end of 28 days while for S_ECC specimens this was on the contrary. The probable reason for ECC specimens to behave in a different manner from each other can be attributed to increased fiber to matrix frictional bond strength and fracture toughness of S_ECC specimens compared to F_ECC specimens which may significantly reduce the chance of multiple crack occurrence and increase the crack widths. In this regard, it can be stated that despite the self-healing performance of S_ECC specimens observed after each number of W/D cycles, the formation of cracks with wider widths due to increased paste maturity and faster consumption of inner materials due to enhanced cementitious behavior suppressed the self-healing occurrence and caused inadequate sealing of cracks which led final RCPT results to increase markedly in the case of S_ECC specimens (see "Crack Characteristics" section). This finding is a strong indication of the dependence of self-healing to tight crack formation and availability of particles to be hydrated. However, it is of great importance to point out that under certain environmental conditioning, even after five repetitive severe pre-load applications, chloride ion penetrability results of both ECC mixtures produced in this study (1798 and 1885 Coulombs for F_ECC and S_ECC, respectively) satisfy low chloride ion penetrability level as prescribed by ASTM C1202 (2002).

4.3 Crack Characteristics

Crack characteristics, which include number of cracks and total crack opening measurements of 3 and 28-day-old ECC specimens subjected to repetitive pre-loading and W/D cycles were summarized in Table 4.2. Data presented in the table were prepared by taking into consideration the average measurements recorded over two opposite faces of three different cylindrical specimens used for RF tests. As seen from Table 4.2, despite the significant self-healing of cracks upon exposure to the subsequent cyclic W/D conditioning with the increase in the number of pre-load applications, both number of cracks and total crack widths increased up to certain level. It can be stated that higher number of cracks were observed in F_ECC specimens compared to S_ECC specimens. Although this characteristic of F_ECC specimens was observed to be true at the end of each pre-load applications and W/D cyclic exposure, it was more explicit for specimens initially cured for 28 days. The probable reasons that might lead F_ECC specimens to show higher number of cracks have already been explained in previous sections and will not be further discussed here.

In Figure 4.3, the rate of total crack closure observed over entire crack surfaces in percentage was given against number of cycles applied to 3 and 28-day-old specimens. When the crack closure rates of 3-day-old ECC specimens exposed to cyclic pre-loading and subsequent W/D conditioning are evaluated, it can be said that comparable self-healing took place in both ECC mixtures although sealing of cracks were slightly better in the case of F_ECC specimens. For specimens initially cured for 28 days however, the total healing of cracks observed over the surface of S_ECC specimens were found to be more pronounced especially during the early ages. The extent of self-healing monitored in the case of 28-day-old S_ECC specimens is rather surprising since the crack widths are larger (Table 4.2) and significantly less undydrated cementitious materials are expected to be present in S_ECC matrices especially at the later ages due to enhanced cementing behavior of slag.

Table 4.2 Crack characteristics of pre-loaded ECC specimens

Mix. ID	# of cycles	3-day-old								28-day-old							
		Pre-loaded				Self-healed				Pre-loaded				Self-healed			
		# of cracks	Crack Width, μm			# of cracks	Crack Width, μm			# of cracks	Crack Width, μm			# of cracks	Crack Width, μm		
		Min.	Max.	Total		Min.	Max.	Total		Min.	Max.	Total		Min.	Max.	Total	
F_ECC	0	7-11	10	100	470	-	-	-	-	5-8	20	110	520	-	-	-	-
	10	8-13	20	100	490	3-9	10	70	280	6-9	20	110	550	3-6	20	80	390
	20	8-14	20	110	530	4-10	20	80	300	6-11	10	120	580	4-7	20	90	450
	30	9-14	20	110	560	6-11	30	80	350	7-11	20	120	630	5-9	30	90	520
	40	10-14	10	110	610	7-12	20	80	390	8-11	20	130	710	7-10	10	110	600
	50	11-14	20	120	640	9-13	20	90	475	9-12	20	130	750	7-11	20	110	680
	60	11-15	10	120	670	9-14	10	100	550	9-12	30	130	790	8-11	20	120	720
	70	12-15	30	120	690	10-14	20	110	590	10-12	20	130	810	9-12	30	120	760
	80	12-16	20	120	710	11-14	20	100	660	10-13	20	140	830	10-12	10	120	790
	90	13-16	20	120	740	11-15	10	100	690	11-13	30	140	860	10-12	20	130	810
S_ECC	0	6-9	20	100	560	-	-	-	-	4-7	20	150	540	-	-	-	-
	10	6-10	10	100	530	3-6	10	60	280	5-8	30	150	570	3-5	20	110	310
	20	7-10	20	110	550	4-8	20	60	310	6-8	30	150	630	4-6	20	120	370
	30	7-10	20	110	580	5-8	10	70	370	6-9	40	150	740	5-7	10	120	570
	40	8-12	20	120	680	6-9	20	90	460	7-9	30	160	780	6-8	30	130	680
	50	9-12	30	120	720	7-10	30	110	580	8-9	20	160	810	7-9	20	130	720
	60	10-12	30	140	880	8-11	10	110	650	8-9	30	180	820	7-9	30	150	770
	70	11-13	30	150	920	9-12	20	110	820	8-9	40	180	890	8-9	20	170	800
	80	11-13	20	150	1010	10-12	10	140	870	8-9	40	200	990	8-9	30	190	870
	90	12-13	20	160	1070	10-12	10	150	980	8-9	40	200	1080	8-9	40	190	980

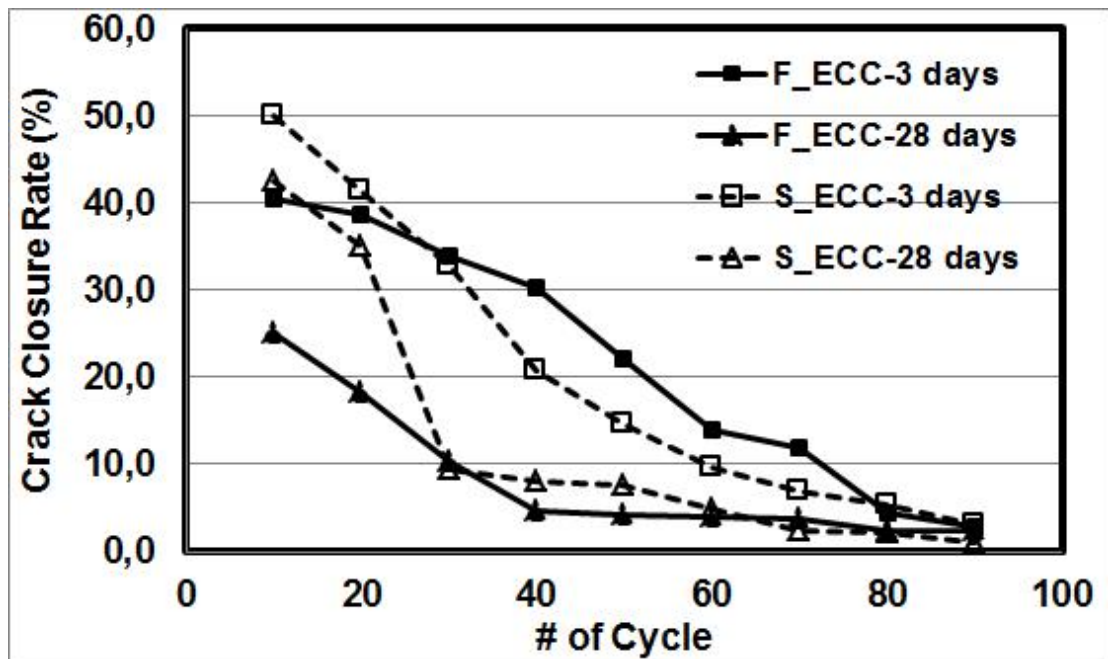


Figure4.3 Total crack closure rates of ECC specimens in percentage

The increased self-healing capability of S_ECC specimens might be associated with high pH value of pore solution which may contribute higher amounts of Ca^{2+} ions to be leached away from C-S-H gels and/or CHs leading to enhanced CaCO_3 growth and final self-healing behavior to be more evident (Sahmaran et al., 2012; Sahmaran and Li, 2010). Although, the higher degree of self-healing was observed in the case of 28-day-old S_ECC specimens, final self-healed condition of specimens was not as complete as F_ECC specimens so that at the end of nine pre-loading and following 90 W/D cycles, total crack opening measured over specimen surfaces were $810 \mu\text{m}$ and $980 \mu\text{m}$ for F_ECC and S_ECC specimens, respectively. This therefore suggests that although self-healing kinetics is faster in bigger cracks (Gagne and Argouges, 2012) availability of required compounds and internal water limit the extent and small crack widths are crucial for complete sealing.

It is of great importance to emphasize that under certain environmental conditioning even after nine repetitive pre-load applications, the maximum individual crack widths observed from 28-day-old specimens were limited to $130 \mu\text{m}$ and $190 \mu\text{m}$ levels for F_ECC and S_ECC specimens, respectively. It must be noted that these values are still below the minimum threshold values reported by different authors for the possibility of complete sealing of a crack (Aldea et al., 2000; Clear, 1985; Edvardsen, 1999). Initial aging of specimens caused differences in repeatability of

crack sealing performance of ECC mixtures. After nine repetitive pre-loading and cyclic W/D exposure, the cracks in 3-day-old specimens were able to be healed from the same place for 4-5 times while in the case of 28-day-old specimens self-healing of same cracks were repeated for 2-3 times, regardless of the SCM type. This situation was monitored to be true for cracks with the widths of no larger than 20 μm and 30 μm in the case of F_ECC and S_ECC specimens, respectively. Moreover, in the cases where the crack widths are restricted to 20-30 μm levels, new cracks that are formed next to healed cracks were observed in some of the situations. Although these cracks were close to former crack sites, due to the availability of unhydrated cementitious materials in opposite crack faces, they were able to be healed rapidly. However, when the widths of cracks started to be larger than approximately 100 μm level, cracks followed to same paths where they were healed at the first place. These results therefore suggest that even under repetitive pre-loading, mechanical recovery is possible although further investigations on related topic are needed to have precise understanding.

CHAPTER 5

CONCLUSIONS

In the present paper, a detailed work was undertaken to have an understanding on the self-healing phenomenon observed in ECC materials in terms of repeatability. From the test results and analysis of self-healed ECC specimens incorporating different SCMs (i.e Class-F fly ash and slag), the following conclusions can be drawn:

- Regardless of the point of measurement, the recovery of RF measurements started to stabilize after around six pre-load applications and subsequent 60 W/D cycles for 3-day-old ECC specimens. In the case of 28-day-old ECC specimens, however, stabilization in RF recovery results started after the application of around three repetitive pre-load applications and following 30 W/D cycles. It can be deduced from the results that depending on the type of SCM used and initial curing time, recovery rate in RF measurements might reach up to 85% of the initial measurement even after six repetitive pre-loading.
- For measurements taken from the middle portion of specimens, RF recovery rates were observed to be lower compared to measurements taken from surface in all the cases, which was attributed to the inconvenience of moisture to diffuse to longer distances. Although, the RF recovery results have dropped in the case of middle-portion measurements, the number of recovered pre-load applications stayed the same as in top-portion measurements with slightly lower recovery rates. These findings show that even under repetitive loading conditions, self-healing mechanism is widely dispersive over the entire area of the specimens rather than being limited in specific regions although the extent of it is highly dependent on the cracks to be easily exposed to water.

- After the application of nine repetitive pre-loading, different crack frequencies were observed over the specimens. Higher number of cracks having narrower widths was observed in the case of F_ECC specimens compared to S_ECCs. Although, there was an increase in number of cracks and crack widths after the pre-loading, the maximum crack widths for F_ECC and S_ECC specimens after the application of nine repetitive pre-loading and following 90 W/D cycles were 130 μm and 190 μm , respectively.

REFERENCES

- ACI Committee 116R. (1994). Cement and concrete terminology. ACI manual of concrete practice.
- ACI Committee 318R (2002). Building Code Requirements for Structural Concrete and Commentary. American Concrete Institute, Farmington Hills, Michigan, pp. 443
- Ahn, T. H. (2008). Development of self-healing concrete incorporating geomaterials: a study on its mechanism and behavior in cracked concrete. PhD dissertation, Department of Civil Engineering, The University of Tokyo, Japan.
- Ahn, T. H. and Kishi, T. (2008). The effect of geomaterials on the autogenous healing behavior of cracked concrete. *Proceeding of 2nd ICCRRR*, Cape Town, South Africa, p. 235–40
- Ahn, T. H. and Kishi, T. (2010). Crack self-healing behavior of cementitious composites incorporating various mineral admixtures. *Advanced Concrete Technology*, **8** (2), 171–86.
- Aldea, C., Song, W., Popovics, J. S. and Shah, S. P. (2000). Extent of healing of cracked normal strength concrete. *Materials in Civil Engineering*, **12**, 92-96.
- ASTM C215. (2008). Standard test method for fundamental transverse, longitudinal, and torsional resonant frequencies of concrete specimens. *American Society for Testing Materials*.
- ASTM Standard C1202. (2002). Standard test method for electrical indication of concrete's ability to resist chloride ion penetration. In: , Philadelphia, PA, USA.

ASTM Standard C618. (2003). Standard specification for coal fly ash and/or calcined natural pozzolan for use in concrete. American society for testing and materials. West Conshohocken, PA, USA.

ASTM Standard C989. (2009). Standard specification for slag cement for use in concrete and mortars. American society for testing and materials. West Conshohocken, PA, USA.

Boh, B. and Sumiga, B. (2008). Microencapsulation technology and its applications in building construction materials. *Materials and Geoenvironment*, **55** (3), 329–344.

Clear, C. A. (1985). The effects of autogenous healing upon the leakage of water through cracks in concrete, *Cement and Concrete Association*, Wexham Springs, p. 28.

Dry, C. and McMillan, W. (1996). Three-part methylmethacrylate adhesive system as an internal delivery system for smart responsive concrete. *Smart Materials and Structures*, **5** (3), 297–300.

Edvardsen, C. (1999). Water permeability and autogenous healing of cracks in concrete. *ACI Materials Journal*, **96** (6), 448–55.

Gagne, R. and Argouges, M. (2012). A study of the natural self-healing of mortars using air-flow measurements. *Materials and Structures*, **45** (11), 1625–1638.

Glanville, W. H. (1931). The permeability of portland cement concrete. Technical Paper, *Building Research*, **3**, 1–61.

Glasser, F. P. (1991). Chemical, mineralogical, and microstructural changes occurring in hydrated slag-cement blends. *Materials Science of Concrete II*, The American Ceramic Society, Inc., Loc., pp. 41–81.

Gollapudi, U. K., Knutson, C. L., Bang, S. S. and Islam, M. R. (1995). A new method for controlling leaching through permeable channels. *Chemosphere*, **30**, 695–705.

Hearn, N. (1999). Effect of shrinkage and load-induced cracking on water permeability of concrete. *ACI Materials Journal*, **96** (2), 234–241.

Hearn, N. and Morley, C. T. (1997). Self-healing property of concrete – experimental evidence. *Materials and Structures*, **30**, 404-411.

Hearn, N. and Morley, C. T. (1998). Self-healing, autogenous healing and continued hydration: what is the difference? *Materials and Structures*, **31**, 563–567.

Hemsley, A. R., Griffiths, P. C. (2000). Architecture in the microcosm: biocolloids, self-assembly and pattern formation. *Philosophical Transactions of the Royal Society*, **358**, 547–64.

Homma, D., Mihashi, H. and Nishiwaki, T. (2009). Self-healing capability of fibre reinforced cementitious composites. *Advanced Concrete Technology*, **7** (2), 217–28.

Huang, H. and Ye, G. (2011). Application of sodium silicate solution as self-healing agent in cementitious materials. *International Conference on Advances in Construction Materials through Science and Engineering*, Hong Kong, China, September 5–7.

Hyde, G. W. and Smith, W. J. (1889). Results of experiments made to determine the permeability of cements and cement mortars. *Journal of the Franklin Institute*, 199–207.

Jacobsen, S. and Sellevold, E. J. (1996). Self-healing of high strength concrete after deterioration by freeze/thaw. *Cement and Concrete Research* **26** (1), 55–62.

Jacobsen, S., Marchand, J. and Homain, H. (1995). SEM observations of the microstructure of frost deteriorated and self-healed concrete. *Cement and Concrete Research*, **25**, 1781-1790.

Jiang, Z., Sun, Z. and Wang, P. (2006). Internal relative humidity distribution in high-performance cement paste due to moisture diffusion and self desiccation. *Cement and Concrete Research*, **36** (2), 320-325.

Jonkers, H. M. (2011). Bacteria-based self-healing concrete. *HERON*, **56**, 1/2.

Jonkers, H. M., Thijssen, A., Muyzer, G., Copuroglu, O. and Schlangen, E. (2008). Application of Bacteria As Self-Healing Agent for the Development of Sustainable

Concrete. *Proceedings of the 1st international conference on biogeocivil engineering*, Delft, The Netherlands.

Joseph, C., Jefferson, A. D. and Cantoni, M. B. (2007). Issues relating to the autonomic healing of cementitious materials. *Proceedings of first international conference on self-healing materials*, Noordwijkaan Zee, Netherlands. Paper 61.

Joseph, C., Jefferson, A. D., Isaacs, B., Lark, R. and Gardner, D. (2010). Experimental investigation of adhesive-based self-healing of cementitious materials. *Magazine of Concrete Research*, **62** (11), 831-843

Kim, Y. Y., Kong, H. J. and Li, V. C. (2003). Design of Engineered Cementitious Composite (ECC) suitable for wet-mix shotcreting. *ACI Materials Journal*, **100**, 511-518.

Kishi, T., Ahn, T. H., Hosoda, A and Takaoka, H. (2007). Self-healing behavior by cementitious recrystallization of cracked concrete incorporating expansive agent. *First International Conference on Self-Healing Materials*, The Netherlands, April 18–20.

Kong, H. J., Bike, S. and Li, V.C. (2003). Development of a Self-Consolidating Engineered Cementitious Composite Employing Electrosteric Dispersion/Stabilization. *Cement and Concrete Composites*, **25**, 301-309.

Kosmatka, S. H. and Panarese, W. C. (1988). Design and control of concrete mixtures. *Thirteenth ed. Portland Cement Association*, Skokie, IL pp.205.

Lepech, M. and Li, V. C. (2008). Large Scale Processing of Engineered Cementitious Composites. *ACI Materials Journal*, **105** (4), 358-366.

Li, V. C. (1997). Engineered cementitious composites tailored composites through micromechanical modeling. *Fiber Reinforced Concrete: Present and the Future*, Banthia, N. A., Bentur and Mufti, A. Editor, pp. 64-97.

- Li, V. C. (1998). ECC – tailored composites through micromechanical modeling. *Fiber Reinforced Concrete: Present and the Future*, Banthia et al., CSCE, Montreal, (1998), pp. 64-97.
- Li, V. C. (2003). On Engineered Cementitious Composites (ECC) – A review of the material and its applications. *Advanced Concrete Technology*, **1** (3) (2003), pp. 215-230.
- Li, V. C. and Herbert, E. (2012). Robust self healing concrete for sustainable infrastructure. *Advanced Concrete Technology*, **10**, 207–218.
- Li, V. C., Lim, Y. M. and Chan, Y. (1998). Feasibility study of a passive smart self-healing cementitious composite. *Composites Part B: Engineering*, **29B**, 819-827.
- Li, V. C., Wang, S. and Wu, C. (2001). Tensile strain-hardening behavior of PVA-ECC. *ACI Materials Journal*, **98** (6), 483-492.
- Li, V. C. and Leung, C. K. Y. (1992). Theory of steady state and multiple cracking of random discontinuous fiber reinforced brittle matrix composites. *ASCE Journal of Engineering Mechanics*, **118**, 2246–2264.
- Lin, Z. and Li, V. C. (1997). Crack bridging in fiber reinforced cementitious composites with slip-hardening interfaces. *Mechanics and Physics of Solids*, **45**, 763-787.
- Lin, Z., Kanda, T. and Li, V. C. (1999). On interface property characterization and performance of fiber reinforced cementitious composites. *Concrete Science and Engineering*, **1**, 173-184.
- Maalej, M., Hashida, T. and Li, V. C. (1995). Effect of fiber volume fraction on the off-crack plane energy in strain-hardening engineered cementitious composites. *American Ceramic Society*, **78** (12), 3369–75.
- Marshall, D. B. and Cox, B. N. (1988). A J-integral method for calculating steady-state matrix cracking stresses in composites. *Mechanics of Materials*, **8**, 127–133.

Mather, B. and Warner, J. (2003). Why do concrete repairs fail, interview held at University of Wisconsin, Department of Engineering Professional Development, Wis. <http://aec.engr.wisc.edu/resources/rsrc07.html>>.

Mihashi, H., Kaneko, Y., Nishiwaki, T. and Otsuka, K. (2000). Fundamental study on development of intelligent concrete characterized by self-healing capability for strength, *Japan Concrete Institute* **22** (2), 441–50.

Moranville-Regourd, M. (1998). Cements made from blast furnace slag, *Lea's Chemistry of Cement and Concrete*, 4th Edition, P. C. Hewlett Ed., Arnold, London, pp. 663-674.

Neville, A. M. (1996). Properties of Concrete. Fourth Edition, John Wiley & Sons, New York, pp. 884.

Neville, A. M. (2002). Autogenous healing – a concrete miracle. *Concrete International* November: 76–82.

Nishiwaki, T. (1997). Fundamental study on development of intelligent concrete with self-healing capability. Master's thesis, Tohoku University.

Qian, S., Zhou, J., de Rooij, M. R. (2009). Self-healing behavior of strain hardening cementitious composites incorporating local waste materials. *Cement and Concrete Composites*, **31**, 613–21.

Rattner, E. (2011). Cost-effective self-healing concrete. <<http://thefutureofthings.com/news/10104/cost-effective-self-healing-concrete.html>>.

Reinhardt, H. and Jooss, M. (2003). Permeability and self-healing of cracked concrete as a function of temperature and crack width. *Cement and Concrete Research*, **33**, 981-985.

Roy, D.M. (1992). The effect of blast furnace slag and related materials on the hydration and durability of concrete. *G. M. Idorn International Symposium*, SP-131, J. Holman and M. Geiker, Eds., American Concrete Institute, Detroit, Michigan, pp. 195-208.

Sahmaran, M and Li, V. C. (2007). De-icing salt scaling resistance of mechanically loaded Engineered Cementitious Composites. *Cement and Concrete Research*, **37** (7), 1035-1046.

Sahmaran, M. and Li, V. C. (2010). Engineered Cementitious Composites: Can They Be Accepted as a Crack-Free Concrete? *Journal of Transportation Research Record*, **39** (11), 1033-1043.

Sahmaran, M., Yildirim, G. and Erdem, T. K. (2012). Self-healing capability of cementitious composites incorporating different supplementary cementitious materials. *Cement and Concrete Composites*, **35** (1), 89-101.

Sahmaran, M., Yucel, H. E. Demirhan, S., Arik, M. T. and Li, V. C. (2012). Combined effect of aggregate and mineral admixtures on tensile ductility of Engineered Cementitious Composites. *ACI Materials Journal*, **109** (6), 627-638.

Schlangen E. (2010). Fracture mechanics. CT5146 Lecture Notes. In: Hua X. Self-healing of engineered cementitious composites (ECC) in concrete repair system. Master thesis, Delft University of Technology.

Schleicher, L. and Green, B. K. (1956). Manifold record material. US patent 2730456.

Shehata, M. H., Thomas, M. D. A and Bleszynski, R. F. (1999). The effect of fly ash composition on the chemistry of pore solution. *Cement and Concrete Research*, **29** (12) 1915–1920.

Song, G. and van Zijl, G. P. A. G (2004). Tailoring ECC for commercial application. *6th Int. RILEM Symposium on Fiber Reinforced Concrete, RILEM Pro039*, pp. 1391–1400.

Stang, H. and Li, V.C. (1999). Extrusion of ECC-material. *In Proc. Of High Performance Fiber Reinforced Cement Composites 3 (HPFRCC 3)* edited by H. Reinhardt and A. Naaman, Chapman & Hull, pp. 203-212.

Stark, J. and Ludwig, H. M. (1997). Influence of water quality on the frost resistance of concrete. *Freeze-Thaw Durability of Concrete*, J. Marchand, M. Pigeon, and M. Setzer Eds., E & FN Spon, London, pp. 157-164.

Taylor, H. F. W. (1997). *Cement Chemistry*, Second Edition. Thomas Telford Publishing, London, pp. 459.

Thao, T. D. P., Johnson, T. J. S., Tong, Q. S. and Dai, P. S. (2009). Implementation of self-healing in concrete – proof of concept. *The IES Journal Part A: Civil and Structural Engineering*, **2** (2), 116–25.

van der Zwaag S. (2010). Routes and mechanisms towards self-healing behavior in engineering materials. *Bulletin of the Polish Academy of Sciences*, **58** (2), 227–36.

van Tittelboom, K., de Belie, N., Muynck, W. D. and Verstraete, W. (2010). Use of bacteria to repair cracks in concrete. *Cement and Concrete Research*, **40**, 157–66.

van Tittelboom, K., De Belie, N., van Loo, D. and Jacobs, P. (2011). Self-healing efficiency of cementitious materials containing tubular capsules filled with healing agent. *Cement and Concrete Composites*, **33**, 497-505.

Wang, J., van Tittelboom, K., De Belie, N. and Verstraete, W. (2012). Use of silica gel or polyurethane immobilized bacteria for self-healing concrete. *Construction and Building Materials*, **26**, 532-540.

Wang, S. and Li, V. C. (2007). Engineered Cementitious Composites with high-volume fly ash. *ACI Materials Journal*, **104** (3) 233-241.

Wang, S. and Li, V.C. (2004). Tailoring of pre-existing flaws in ECC matrix for saturated strain hardening. *Proceedings of FRAMCOS-5*, Vail, Colorado, USA, pp. 1005–1012.

Weimann, M. B. and Li, V. C. (2003). Hygral behavior of engineered cementitious composites (ECC). *International Journal for Restoration of Buildings and Monuments*, **9**, 513-534.

White, S. R., Sottos, N. R., Geubelle, P. H., Moore, J. S., Kessler, M. R. and Sriram, S. R. (2001). Autonomic healing of polymer composites. *Nature*, **409** (6822), 794.

Wiktor, V. and Jonkers, H. M. (2011).Quantification of crack-healing in novel bacteria-based self-healing concrete.*Cement and Concrete Composites*, **33**, 763-770

Yang, E. H., Yang, Y. and Li, V. C. (2007).Use of high volumes of fly ash to improve ECC mechanical properties and material greenness.*ACI Materials Journal*, **104** (6), 620-628.

Yang, Y. Z., Lepech, M. D., Yang, E. H. and Li, V. C. (2007).Autogenous healing of engineered cementitious composites under wet–dry cycles.*Cement and Concrete Research*, **39**, 382–90.